J|A|C|S
ARTICLES

Hollow Spherical Supramolecular Dendrimers

Virgil Percec,*,† Mihai Peterca,†,‡ Andrés E. Dulcey,† Mohammad R. Imam,†
Steven D. Hudson,§ Sami Nummelin,† Peter Adelman,† and Paul A. Heiney‡

Roy & Diana Vagelos Laboratories, Department of Chemistry, University of Pennsylvania, Philadelphia, Pennsylvania 19104-6323, Department of Physics and Astronomy, University of Pennsylvania, Philadelphia, Pennsylvania 19104-6396, and National Institute of Standards and Technology, Gaithersburg, Maryland 20899-8544

Received May 9, 2008; E-mail: percec@sas.upenn.edu

Abstract: The synthesis of a library containing 12 conical dendrons that self-assemble into hollow spherical supramolecular dendrimers is reported. The design principles for this library were accessed by development of a method that allows the identification of hollow spheres, followed by structural and retrostructural analysis of their $Pm\bar{3}n$ cubic lattice. The first hollow spherical supramolecular dendrimer was made by replacing the tapered dendron, from the previously reported tapered dendritic dipeptide that self-assembled into helical pores, with its constitutional isomeric conical dendron. This strategy generated a conical dendritic dipeptide that self-assembled into a hollow spherical supramolecular dendrimer that self-organizes in a $Pm\bar{3}n$ cubic lattice. Other examples of hollow spheres were assembled from conical dendrons without a dipeptide at their apex. These are conical dendrons originated from tapered dendrons containing additional benzyl ether groups at their apex. The inner part of the hollow sphere assembled from the dipeptide resembles the path of a spherical helix or loxodrome and, therefore, is chiral. The spheres assembled from other conical dendrons are nonhelical, even when they contain stereocenters on the alkyl groups from their periphery. Functionalization of the apex of the conical dendrons with diethylene glycol allowed the encapsulation of LiOTf and RbOTf in the center of the hollow sphere. These experiments showed that hollow spheres function as supramolecular dendritic capsules and therefore are expected to display functions complementary to those of other related molecular and supramolecular structures.

Introduction

Dendrimers and dendrons[1] are monodisperse macromolecules with complex topologies that are synthesized by divergent[2] and convergent[3] iterative methods. They provide some of the most influential building blocks that are currently explored at the interface between chemistry, biology, physics, medicine, and nanoscience.[4] Our laboratory discovered the first spherical supramolecular dendrimers that self-organize in a $Pm\bar{3}n$ cubic lattice previously unencountered in soft matter.[5a] Subsequently, rational design combined with retrostructural analysis was used to establish that this novel cubic periodic array is general for libraries of spherical supramolecular dendrimers[5a−g] derived from self-assembling conical benzyl ether dendrons and from a large variety of other self-assembling conical dendrons with more complex primary structure.[6] The principles of this self-assembly process were investigated by a combination of experiments that include X-ray diffraction (XRD),[5a] transmission electron microscopy (TEM),[7a,b] isomorphous replacement,[7c] advanced NMR methods,[7d] molecular simulations,[7e] and theoretical work.[7f,g] This facilitated the elaboration of design principles for functional spherical supramolecular dendrimers,[8] allowed the transplant of the quasi-equivalence concept from biology to chemistry,[9a] and generated new approaches to controlling chemical reactivity[9b] and other functions. The $Pm\bar{3}n$ cubic

† Department of Chemistry, University of Pennsylvania.
‡ Department of Physics and Astronomy, University of Pennsylvania.
§ National Institute of Standards and Technology.

(1) (a) Fréchet, J. M. J., Tomalia, D. A., Eds. *Dendrimers and Other Dendritic Polymers*; Wiley: New York, 2001. (b) Newkome, G. R.; Moorefield, C. N.; Vögtle, F. *Dendrimers and Dendrons*; Wiley−VCH: Weinheim, Germany, 2001.
(2) (a) Buhleier, E.; Wehner, W.; Vögtle, F. *Synthesis* **1978**, *155*, 158. (b) Tomalia, D. A.; Baker, H.; Dewald, J.; Hall, M.; Kallos, G.; Martin, S.; Roeck, J.; Ryder, J.; Smith, P. *Polym. J.* **1985**, *17*, 117–132. (c) Newkome, G. R.; Yao, Z.; Baker, G. R.; Gupta, V. K. J. *Org. Chem.* **1985**, *50*, 2003–2004.
(3) (a) Hawker, C. J.; Fréchet, J. M. J. *J. Am. Chem. Soc.* **1990**, *112*, 7638–7647. (b) Miller, T. M.; Neenan, T. X. *Chem. Mater.* **1990**, *2*, 346–349.
(4) (a) Moore, J. S. *Acc. Chem. Res.* **1997**, *30*, 402–413. (b) Kim, Y.; Zimmerman, S. C. *Curr. Opin. Chem. Biol.* **1998**, *2*, 733–742. (c) Seebach, D.; Rheiner, P. B.; Greiveldinger, G.; Butz, T.; Sellner, H. *Top. Curr. Chem.* **1998**, *197*, 125–164. (d) Majoral, J.-P.; Caminade, A.-M. *Top. Curr. Chem.* **1998**, *197*, 79–124. (e) Smith, D. K.; Diederich, F. *Chem.—Eur. J.* **1998**, *4*, 1353–1361. (f) Fischer, M.; Vögtle, F. *Angew. Chem., Int. Ed.* **1999**, *38*, 885–905. (g) Bosman, A. W.; Janssen, H. M.; Meijer, E. W. *Chem. Rev.* **1999**, *99*, 1665–1688. (h) Astruc, D.; Chardac, F. *Chem. Rev.* **2001**, *101*, 2991–3024. (i) Haag, R. *Chem.—Eur. J.* **2001**, *7*, 327–335. (j) Hecht, S.; Fréchet, J. M. J. *Angew. Chem., Int. Ed.* **2001**, *40*, 74–91. (k) Tully, D. C.; Fréchet, J. M. J. *Chem. Commun.* **2001**, 1229–1239. (l) Stiriba, S.-E.; Frey, H.; Haag, R. *Angew. Chem., Int. Ed.* **2002**, *41*, 1329–1334. (m) Esfand, R.; Tomalia, D. A. *Drug Discovery Today* **2001**, *6*, 427–436. (n) Gillies, E. R.; Fréchet, J. M. J. *Drug Discovery Today* **2005**, *10*, 35–43. (o) Jiang, D.-L.; Aida, T. *Polym. Prog. Sci.* **2005**, *30*, 403–422. (p) Van de Coevering, R.; Gebbink, R. J. M. K.; Van Koten, G. *Prog. Polym. Sci.* **2005**, *30*, 474–490. (q) Caminade, A.-M.; Majoral, J.-P. *Prog. Polym. Sci.* **2005**, *30*, 491–505. (r) Boas, U.; Heegaard, P. M. H. *Chem. Soc. Rev.* **2004**, *33*, 43–63. (s) Grinstaff, M. W. *Chem.—Eur. J.* **2002**, *8*, 2838–2846. (t) Grayson, S. M.; Fréchet, J. M. J. *Chem. Rev.* **2001**, *101*, 3819–3867.

Scheme 1. Structures of the Library of Conical Dendrons Forming Helical and Nonhelical Supramolecular Hollow Spherical Dendrimers

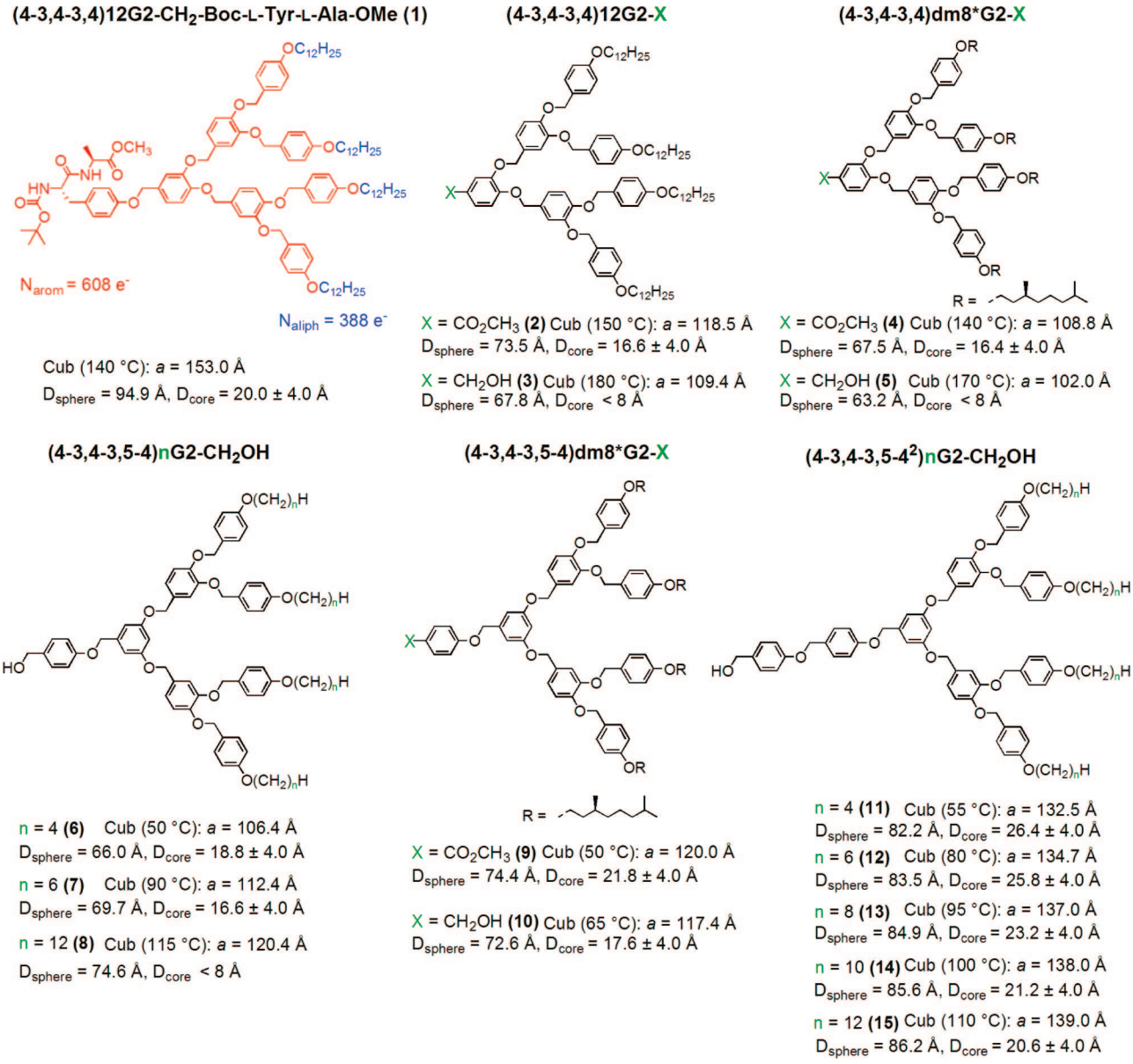

periodic array remains the most widely encountered in libraries of spherical supramolecular dendrimers reported from our[5−8] and other laboratories.[10] However, it has been discovered that conical dendrons self-assemble also in spherical supramolecular structures that self-organize in $Im\bar{3}m$ cubic,[11a,b] $P4_2/mnm$ tetragonal,[11c] and 12-fold liquid quasicrystal quasi-periodic array.[11d] The self-assembly of conical dendrons into spherical supramolecular dendrimers evolved from the assembly of tapered dendrons into cylindrical supramolecular dendrimers.[12] This evolution was facilitated by increasing the generation number[5a] of the dendron, and for the same generation by its primary structure.[5g,6] New functions[8,12] and reactivity principles[9] were provided by the compartmentalization of cylindrical supramolecular dendrimers. Self-assembling dendrons that provide supramolecular spherical dendrimers with the structural perfection that allows their self-organization in lattices are actively investigated also in other laboratories.[1,4,10]

Recently, our laboratory reported the discovery of helical porous supramolecular dendrimers.[13] These assemblies expanded the scope of supramolecular dendrimers into biological mimics with biological functions such as transmembrane channels.[13] Progress on porous supramolecular cylindrical dendrimers relied on the elaboration of new methods of

(5) (a) Balagurusamy, V. S. K.; Ungar, G.; Percec, V.; Johansson, G. *J. Am. Chem. Soc.* **1997**, *119*, 1539–1555. (b) Percec, V.; Cho, W. D.; Mosier, P. E.; Ungar, G.; Yeardley, D. J. P. *J. Am. Chem. Soc.* **1998**, *120*, 11061–11070. (c) Ungar, G.; Percec, V.; Holerca, M. N.; Johansson, G.; Heck, J. A. *Chem.—Eur. J.* **2000**, *6*, 1258–1266. (d) Percec, V.; Cho, W. D.; Möller, M.; Prokhorova, S. A.; Ungar, G.; Yeardley, D. J. P. *J. Am. Chem. Soc.* **2000**, *122*, 4249–4250. (e) Percec, V.; Cho, W. D.; Ungar, G.; Yeardley, D. J. P. *Angew. Chem., Int. Ed.* **2000**, *39*, 1598–1602. (f) Percec, V.; Ahn, C. H.; Cho, W. D.; Jamieson, A. M.; Kim, J.; Leman, T.; Schmidt, M.; Gerle, M.; Möller, M.; Prokhorova, S. A.; Sheiko, S. S.; Cheng, S. Z. D.; Zhang, A.; Ungar, G.; Yeardley, D. J. P. *J. Am. Chem. Soc.* **1998**, *120*, 8619–8631. (g) Percec, V.; Cho, W. D.; Ungar, G. *J. Am. Chem. Soc.* **2000**, *122*, 10273–10281. (h) Percec, V.; Cho, W. D.; Ungar, G.; Yeardley, D. J. P. *J. Am. Chem. Soc.* **2001**, *123*, 1302–1315.

Table 1. Thermal Analysis of the Assemblies Self-Organized from Supramolecular Dendrimers

dendron	thermal transition, °C (corresponding enthalpy change, kcal mol^{-1})[a] heating	cooling
(4-3,4-3,4)12G2-CO_2CH_3 **2**	S 51.2 (7.43) Cub 164.0 (8.41) i Cub 164.0 (8.45) i	i 162.6 (−8.65) Cub
(4-3,4-3,4)12G2-CH_2OH **3**	$\Phi_{r\text{-}s}{}^{o}$ 31.9 (3.95) $\Phi_{r\text{-}s}$ 102.0 (6.46) Cub 188.7 (8.37) i Cub_g 71.2 (−4.47) $\Phi_{r\text{-}s}$ 103.7 (7.19) Cub 188.4 (8.33) i	i 186.9 (−8.58) Cub
(4-3,4-3,4)12G2-CH_2-Boc-L-Tyr-L-Ala-OMe **1**	Cub_g 68.3 (3.67) Cub 149.0 (3.95) i g 56.9 Cub 148.8 (4.01) i	i 147.6 (−3.79) Cub
(4-3,4-3,4)dm8*G2-CO_2CH_3 **4**	Cub 149.8 (7.07) i Cub 149.8 (7.05) i	i 148.1 (−7.16) Cub
(4-3,4-3,4)dm8*G2-CH_2OH **5**	$\Phi_{r\text{-}s}$ 91.6 (1.97) Cub 178.4 (7.60) i Cub 178.1 (7.53) i	i 176.5 (−7.79) Cub
(4-3,4-3,5-4)4G2-CH_2OH **6**	g 37.0 Cub 69.0 (4.40) i g 33.4 Cub 69.0 (4.40) i	i 67.0 (−4.39) Cub 28.6 g
(4-3,4-3,5-4)6G2-CH_2OH **7**	$\Phi_h{}^{g}$ 34.1 (0.45) $\Phi_h{}^{b}$ Cub 88.8 (6.06) i Cub_g 36.0 (0.24) Cub 88.6 (6.01) i	i 87.7 (−6.04) Cub
(4-3,4-3,5-4)12G2-CH_2OH **8**	$\Phi_h{}^{g}$ 40.4 (1.41) $\Phi_h{}^{b}$ Cub 116.5 (6.34) i $\Phi_h{}^{g}$ 36.0 (0.24) $\Phi_h{}^{b}$ Cub 116.3 (6.40) i	i 115.6 (−6.62) Cub
(4-3,4-3,5-4)dm8*G2-CO_2CH_3 **9**	Cub 54.2 (2.74) i Cub 53.2 (2.70) i	i 51.8 (−2.72) Cub
(4-3,4-3,5-4)dm8*G2-CH_2OH **10**	Cub 98.4 (5.25) i Cub 98.4 (5.23) i	i 97.4 (−5.24) Cub
(4-3,4-3,5-4^2)4G2-CH_2OH **11**	g 35.4 Cub 59.8 (4.68) i g 36.7 Cub 59.7 (4.66) i	i 56.9 (−4.78) Cub 32.2 g
(4-3,4-3,5-4^2)6G2-CH_2OH **12**	g 36.7 Cub 83.1 (6.07) i g 36.8 Cub 83.1 (6.07) i	i 81.0 (−6.17) Cub 31.9 g
(4-3,4-3,5-4^2)8G2-CH_2OH **13**	g 42.5 Cub 100.0 (7.12) i g 41.4 Cub 100.0 (7.29) i	i 96.6 (−7.32) Cub 34.8 g
(4-3,4-3,5-4^2)10G2-CH_2OH **14**	g 39.2 Cub 107.2 (7.39) i g 38.7 Cub 106.6 (7.61) i	i 104.0 (−7.52) Cub 32.5 g
(4-3,4-3,5-4^2)12G2-CH_2OH **15**	g 35.5 Cub 112.8 (6.82) i g 36.1 Cub 112.4 (7.32) i	i 110.3 (−7.32) Cub 24.6 g

[a] Data from the first heating and cooling DSC scans (10 °C min^{-1}) are on the first line, and data from the second heating are on the second line, for each dendron. S, smectic phase; $\Phi_{r\text{-}s}{}^{o}$, ordered simple rectangular columnar lattice; Cub_g, glassy cubic phase; $\Phi_h{}^{g}$, glassy hexagonal columnar phase; $\Phi_{r\text{-}s}$, *p2mm* simple rectangular columnar LC phase; Φ_h, *p6mm* hexagonal columnar LC phase; Cub, $Pm\bar{3}n$ cubic lattice; g, glass; i, isotropic. [b] Phase observed only in XRD.

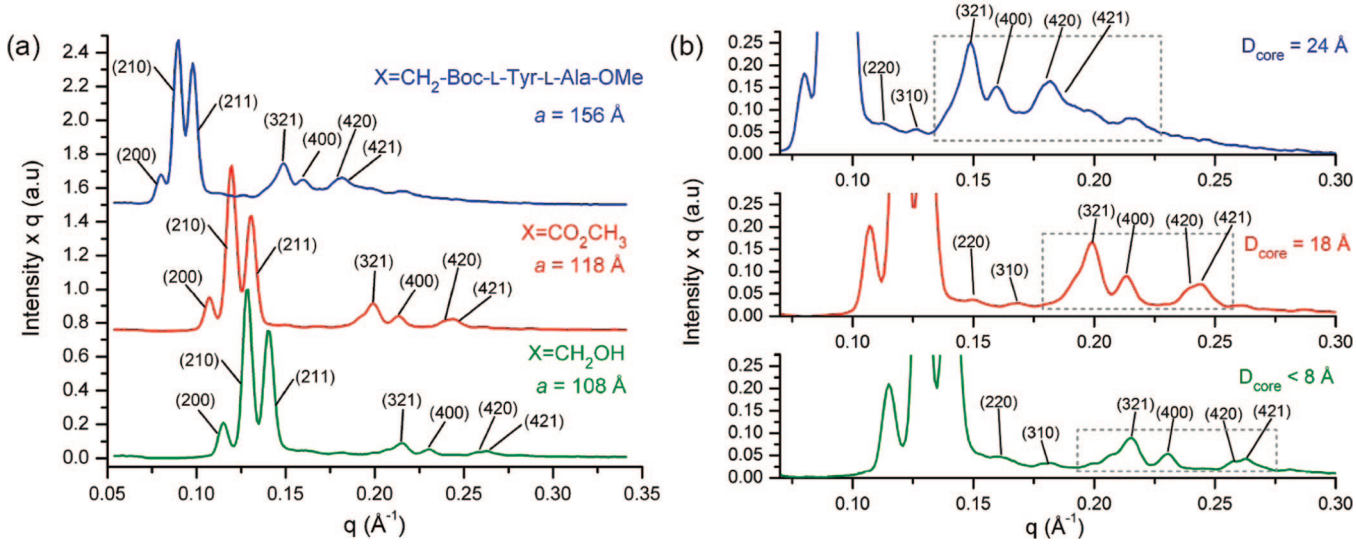

Figure 1. (a) Small-angle powder XRD plots of the (4-3,4-3,4)12G2-X dendrons in the $Pm\bar{3}n$ cubic phase. (b) Expansion of the plots showing the gradual increase in relative intensities of the peaks marked by the dotted rectangles. Lattice parameter *a*, diffraction peaks indexing, and the calculated hollow center diameters (D_{core}) are indicated.

porous structure detection and computation based on the structural information from XRD experiments.[13f] The detection of porous structures self-assembled from alkyl-substituted dendrons was signaled by the enhanced amplitude of higher-order diffraction peaks in the columnar hexagonal (Φ_h)[13a] and rectangular ($\Phi_{r\text{-}s}$, $\Phi_{r\text{-}c}$)[13f] phases. Pore diameter was calculated by reconstruction of the powder XRD.[13a,f] Subsequently, a combination of methods based on small- and wide-angle powder and fiber XRD experiments together with TEM, electron diffraction (ED) experiments, electron density maps, and simulation of XRD was developed and used to reconstruct the 3-D structure of the porous supramolecular column.[13a] The porous structure determined by XRD experiments[13a] was supported by transport experiments.[13a,j]

Table 2. XRD Powder Data and Structural Analysis of Supramolecular Dendrimers

dendron	T (°C)	phase	a, b[a] (Å)	d-spacings[b] (Å)
(4-3,4-3,4)12G2-CO_2CH_3 **2**	26	smectic[c,d]	54.9	55.0, 27.5
	150	$Pm\bar{3}n$[e]	118.5	59.2 [16.4], 52.9 [18.3], 48.4 [16.4], 32.9 [5.6], 31.6 [6.5], 29.6 [12.7]
(4-3,4-3,4)dm8*G2-CO_2CH_3 **4**	145	$Pm\bar{3}n$[e]	108.8	54.2 [13.3], 48.7 [14.6], 44.5 [13.9], 32.9 [5.0], 31.6 [5.9], 29.6 [14.6]
(4-3,4-3,4)12G2-CH_2OH **3**	98	$p2mm$[f]	89.7, 49.3	49.3, 44.8, 43.2, 29.9, 25.6, 24.6, 22.4, 21.6, 16.9
	180	$Pm\bar{3}n$[e]	109.4	54.7, 48.9, 44.7, 30.3, 29.2, 27.4
(4-3,4-3,4)dm8*G2- CH_2OH **5**	65	$p2mm$[d,f]	84.7, 46.3	46.3, 42.3, 40.7, 28.3, 24.1, 23.2, 21.2, 20.3, 15.9
	170	$Pm\bar{3}n$[e]	102.0	51.0, 45.6, 41.6, 28.3, 27.3, 25.5
(4-3,4-3,4)12G2-CH_2-Boc-L-Tyr-L-Ala-OMe **1**	140	$Pm\bar{3}n$[e]	153	76.5 [10.1], 68.4 [12.2], 62.5 [11.7], 42.4 [6.4], 40.9 [6.7], 38.3 [13.9]
(4-3,4-3,5-4)4G2-CH_2OH **6**	50	$Pm\bar{3}n$[e]	106.4	52.9 [9.4], 47.6 [12.4], 43.6 [11.6], 29.5 [6.5], 28.6 [6.8], 26.6 [16.7]
(4-3,4-3,5-4)6G2-CH_2OH **7**	25	$p6mm$[g]	55.3	48.1 [40.8], 27.6 [28.0], 23.9 [21.0], 18.1 [10.1]
	88	$Pm\bar{3}n$[e]	112.4	56.2 [9.7], 50.3 [14.5], 45.9 [13.2], 31.2 [6.9], 30.0 [6.6], 27.3 [16.4]
(4-3,4-3,5-4)dm8*G2-CO_2CH_3 **9**	50	$Pm\bar{3}n$[e]	120.0	60.1 [11.6], 53.7 [13.1], 49.0 [12.5], 33.3 [7.7], 32.1 [8.7], 30.0 [15.5]
(4-3,4-3,5-4)dm8*G2-CH_2OH **10**	65	$Pm\bar{3}n$[e]	117.4	58.2 [13.9], 52.6 [14.9], 48.4 [14.8], 32.5 [5.9], 31.4 [6.1], 29.3 [15.1]
(4-3,4-3,5-4)12G2-CH_2OH **8**	30	$p6mm$[g]	62.6	54.3, 31.4, 27.2
	115	$Pm\bar{3}n$[e]	120.4	60.2, 53.8, 49.2, 33.4, 32.2, 30.1
(4-3,4-3,5-4^2)4G2-CH_2OH **11**	55	$Pm\bar{3}n$[e]	132.5	66.3 [8.7], 59.3 [10.7], 54.1 [9.9], 36.7 [5.0], 35.4 [5.2], 33.1 [17.3]
(4-3,4-3,5-4^2)6G2-CH_2OH **12**	80	$Pm\bar{3}n$[e]	134.7	67.3 [8.6], 60.2 [10.6], 54.9 [9.8], 37.2 [4.9], 36.0 [5.2], 33.6 [16.1]
(4-3,4-3,5-4^2)8G2-CH_2OH **13**	95	$Pm\bar{3}n$[e]	137	68.5 [10.1], 61.2 [12.6], 55.9 [11.7], 37.9 [5.7], 36.6 [5.8], 34.2 [13.2]
(4-3,4-3,5-4^2)10G2-CH_2OH **14**	100	$Pm\bar{3}n$[e]	138	69.0 [10.9], 61.7 [13.6], 53.4 [12.7], 38.3 [5.1], 36.9 [6.4], 34.5 [14.2]
(4-3,4-3,5-4^2)12G2-CH_2OH **15**	110	$Pm\bar{3}n$[e]	139	69.5 [13.9], 62.1 [15.6], 56.7 [13.7], 38.6 [5.1], 37.1 [6.2], 34.8 [11.3]

[a] Lattice parameter a is listed for $p6mm$ and $Pm\bar{3}n$ phases; both parameters a and b are given for $p2mm$ phases. [b] d-spacings and peak scaled relative amplitudes [in brackets] were calculated from the equation $A_{hkl} = (q_{hkl}\text{area}_{hkl}/m_{hkl})^{1/2}/\sum_{mnp}(q_{mnp}\text{area}_{mnp}/m_{mnp})^{1/2}$, where q_{hkl} is peak position, area_{hkl} = peak area, m_{hkl} is peak multiplicity, and the sum was performed for all observed X-ray diffraction peaks. [c] For the smectic phase, d_{10} and d_{20} spacings are listed. They have the ratio 1:2, and $a = (d_{10} + 2d_{20})/2$. [d] Phase observed only in the first heating of the as-prepared sample. [e] For $Pm\bar{3}n$ phases, d_{200}, d_{210}, d_{211}, d_{320}, d_{321}, and d_{400} spacings are listed. They have the ratio $\sqrt{4}:\sqrt{5}:\sqrt{6}:\sqrt{13}:\sqrt{14}:\sqrt{16}$, and $a = (\sqrt{4}d_{200} + \sqrt{5}d_{210} + \sqrt{6}d_{211} + \sqrt{13}d_{320} + \sqrt{14}d_{321} + \sqrt{16}d_{400})/6$. A_{hkl} values are shown in brackets. [f] For $p2mm$ phases, d_{01}, d_{20}, d_{11}, d_{30}, d_{31}, d_{02}, d_{40}, d_{22}, and d_{51} spacings are listed. The ratio of the peaks is calculated from the equation $d_{hk} = [(h/a)^2 + (k/b)^2]^{-1/2}$; $a = (2d_{20} + 3d_{30} + 4d_{40})/3$ and $b = d_{01}$. [g] For $p6mm$ phases, d_{10}, d_{11}, d_{20}, and d_{21} spacings are listed. They have the ratio $1:\sqrt{3}:\sqrt{4}:\sqrt{7}$, and $a = 2/\sqrt{3}\ d_{10} + \sqrt{3}d_{11} + 2d_{20} + \sqrt{7}d_{21}/4$. A_{hk} values are shown in brackets.

In a previous publication we discussed the potential XRD signature of supramolecular spherical clusters containing a less dense center.[14] In this paper, a rational approach to the design of hollow spherical supramolecular dendrimers that self-organize in a $Pm\bar{3}n$ cubic periodic array, as well as a method for potential identification of hollow spheres and calculation of the dimensions of the hollow core of the supramolecular sphere by reconstruction of the XRD data, is presented. Mechanisms for the assembly of helical and nonhelical supramolecular hollow spheres are discussed. Preliminary results on the encapsulation of LiOTf and RbOTf in the center of a hollow sphere containing a diethylene glycol binding motif at the apex of the dendron are also presented.

Results and Discussion

Synthesis, Thermal Analysis, and Rational Selection of Conical Dendrons That Self-Assemble into Hollow Spheres. Scheme 1 outlines the conical dendritic structures that were designed to self-assemble into hollow spherical supramolecular dendrimers. Their synthesis was carried out by synthetic strategies elaborated previously in our laboratory.[5g,13a] Synthetic details are available in the Supporting Information. A combination of ^{1}H and ^{13}C NMR, HPLC, and matrix-assisted laser desorption ionization time-of-flight (MALDI-TOF) mass spectrometry techniques was used to demonstrate the chemical structure and purity (>99%) of all intermediary and final compounds. Thermal analysis of the supramolecular assemblies was performed by differential scanning calorimetry (DSC) and the phase assignment was accomplished by XRD. The principles used for selection of these dendrons were elaborated by various combinations of experiments. Previously we discovered that the tapered dendritic dipeptide (4-3,4-3,5)12G2-CH_2-Boc-L-Tyr-L-Ala-OMe[13a] self-assembled into helical porous columns. However, the precursor to this dendritic dipeptide, (4-3,4-3,5)12G2-CH_2OH, self-assembled into nonporous helical columns.[5g,13a,e] Therefore, the attachment of the dipeptide to a tapered dendron maintained the shape of the supramolecular assembly resulting from the parent dendron. Nevertheless, attachment of the dipeptide to the apex of the tapered dendron induced a porous structure and selected the helix sense of the already helical column. The constitutional isomeric dendron (4-3,4-3,4)12G2-CH_2OH (**3**) self-assembled into nonhollow supramolecular spheres.[5g] Therefore, the question that provided the working hypothesis for the current experiments was, will the attachment of the same dipeptide at the apex of the conical (4-3,4-3,4)12G2-CH_2-X dendron, by analogy with the case of its tapered constitutional isomer,[13a] induce the assembly of a hollow sphere? If the answer to this question was yes, a second question would emerge. Will the resulting hollow sphere be helical and therefore chiral? As will be demonstrated later, the answer to both

(6) (a) Percec, V.; Mitchell, C. M.; Cho, W. D.; Uchida, S.; Glodde, M.; Ungar, G.; Zeng, X. B.; Liu, Y. S.; Balagurusamy, V. S. K.; Heiney, P. A. *J. Am. Chem. Soc.* **2004**, *126*, 6078–6094. (b) Percec, V.; Peterca, M.; Sienkowska, M. J.; Ilies, M. A.; Aqad, E.; Smidrkal, J.; Heiney, P. A. *J. Am. Chem. Soc.* **2006**, *128*, 3324–3334. (c) Percec, V.; Holerca, M. N.; Nummelin, S.; Morrison, J. L.; Glodde, M.; Smidrkal, J.; Peterca, M.; Rosen, B. M.; Uchida, S.; Balagurusamy, V. S. K.; Sienkowska, M. J.; Heiney, P. A. *Chem.—Eur. J.* **2006**, *12*, 6216–6241.

(7) (a) Hudson, S. D.; Jung, H. T.; Percec, V.; Cho, W. D.; Johansson, G.; Ungar, G.; Balagurusamy, V. S. K. *Science* **1997**, *278*, 449–452. (b) Hudson, S. D.; Jung, H. T.; Kewsuwan, P.; Percec, V.; Cho, W. D. *Liq. Cryst.* **1999**, *26*, 1493–1499. (c) Dukeson, D. R.; Ungar, G.; Balagurusamy, V. S. K.; Percec, V.; Johansson, G. A.; Glodde, M. J. *Am. Chem. Soc.* **2003**, *125*, 15974–15980. (d) Rapp, A.; Schnell, I.; Sebastiani, D.; Brown, S. P.; Percec, V.; Spiess, H. W. *J. Am. Chem. Soc.* **2003**, *125*, 13284–13297. (e) Li, Y. Y.; Lin, S. T.; Goddard, W. A., III *J. Am. Chem. Soc.* **2004**, *126*, 1872–1885. (f) Ziherl, P.; Kamien, R. D. *Phys. Rev. Lett.* **2000**, *85*, 3528–3531. (g) Ziherl, P.; Kamien, R. D. *J. Phys. Chem. B* **2001**, *105*, 10147–10158.

(8) (a) Percec, V.; Holerca, M. N.; Uchida, S.; Cho, W. D.; Ungar, G.; Lee, Y. S.; Yeardley, D. J. P. *Chem.—Eur. J.* **2002**, *8*, 1106–1117. (b) Percec, V.; Cho, W. D.; Ungar, G.; Yeardley, D. J. P. *Chem.—Eur. J.* **2002**, *8*, 2011–2025.

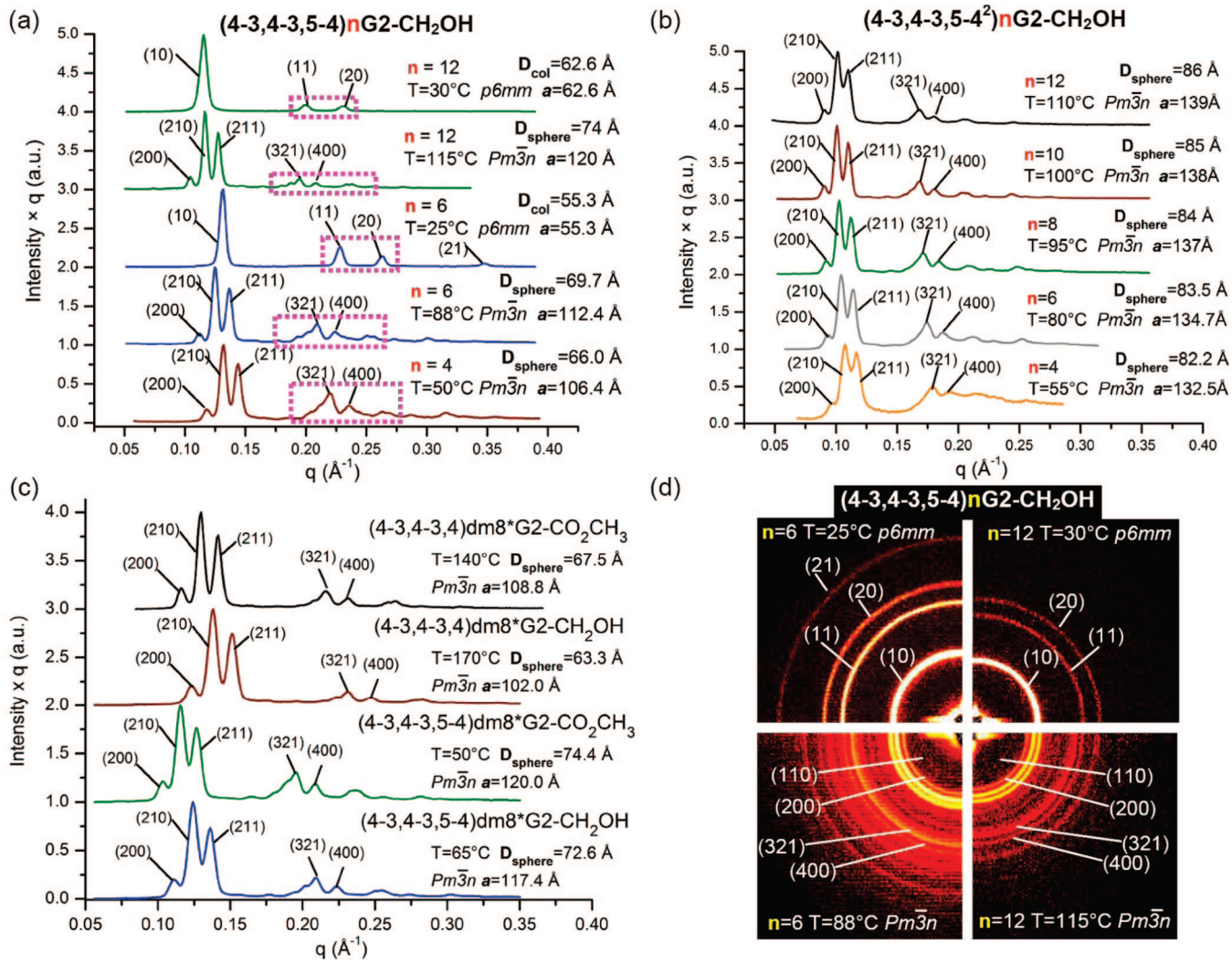

Figure 2. Small-angle XRD powder plots of (a) (4-3,4-3,5-4)*n*G2CH$_2$OH with $n = 4$, 6, or 12 (compounds **6**−**8**); (b) (4-3,4-3,5-4^2)*n*G2CH$_2$OH with $n =$ 4, 6, 8, 10, or 12 (compounds **11**−**15**); and (c) (4-3,4-3,4)dm8*G2-X and (4-3,4-3,5-4)dm8*G2-X with X = CO_2CH_3 or CH_2OH (compounds **4**, **5**, **9**, and **10**). (d) Comparative XRD patterns for (4-3,4-3,5-4)*n*G2CH$_2$OH with $n = 6$ (**7**) or 12 (**8**) in their Φ_h (*p6mm*) and cubic (*Pm*$\bar{3}$*n*) phases. The lattice parameters (*a*), column diameter (D_{col}), sphere diameter (D_{sphere}), and temperatures are indicated; dotted rectangles in panel a indicate enhancement of the higher-order diffraction peak amplitudes for both hexagonal and cubic phases for $n = 4$ or 6; the enhancement is visible also in panel d.

questions was yes, and therefore, related principles were used for the design of the other dendrons shown in Scheme 1.

Subsequently, we investigated the structure of supramolecular spheres generated from the parent dendrons (4-3,4-3,4)12G2-X with X = CO_2CH_3 (**2**) and CH_2OH (**3**), and we discovered that in the case of **2** a hollow sphere was assembled, while in the case of **3** a nonhollow sphere was generated (Table 1). This observation could not have been made before since no analytical methods to identify and calculate the structure and the dimensions of a hollow sphere were available.[5g] The discovery of the helical hollow sphere via the dendritic dipeptide concept prompted us to investigate the induction of helicity into the hollow sphere self-assembled from **2** and **3** by the incorporation of stereocenters in the alkyl groups of the dendrons (4-3,4-3,4)dm8*G2-X with X = CO_2CH_3 (**4**) and CH_2OH (**5**). Hollow spheres were assembled, but the spherical supramolecular structures obtained were not chiral. This suggests that the dipeptide from the apex of the conical dendron must be involved in generation of the helical structure.

Earlier experiments demonstrated[5,6c,13a] that incorporation of alternative bulky substituents (other than a dipeptide) into the apex of the dendron induced the formation of porous columns. Attempts to generate porous columnar assemblies from the attachment of one and two benzyl ethers at the apex of (4-3,4-3,5)*n*G2-X, and incorporation of stereocenters on the alkyl groups from their periphery, produced (4-3,4-3,5-4)*n*G2-X with $n = 4$ (**6**), 6 (**7**), and 12 (**8**) (Scheme 1); (4-3,4-3,5-4)dm8*G2-X with X = CO_2CH_3 (**9**) and CH_2OH (**10**) (Scheme 1); and (4-3,4-3,5-4^2)*n*G2-CH$_2$OH with $n = 4$ (**11**), 6 (**12**), 8 (**13**), 10 (**14**), and 12 (**15**) (Scheme 1); all of which self-assemble into hollow spheres. Expansion of the apex functional group, while it maintains an identical outer aromatic substitution pattern, favored the formation of spherical assemblies via the change in dendron conformation from tapered to conical (Figure SF10 in Supporting Information).

(9) (a) Percec, V.; Ahn, C. H.; Ungar, G.; Yeardley, D. J. P.; Möller, M.; Sheiko, S. S. *Nature* **1998**, *391*, 161–164. (b) Percec, V.; Ahn, C. H.; Barboiu, B. *J. Am. Chem. Soc.* **1997**, *119*, 12978–12979. (c) Percec, V.; Holerca, M. N. *Biomacromolecules* **2000**, *1*, 6–16. (d) Percec, V.; Holerca, M. N.; Magonov, S. N.; Yeardley, D. J. P.; Ungar, G.; Duan, H.; Hudson, S. D. *Biomacromolecules* **2001**, *2*, 706–728. (e) Percec, V.; Holerca, M. N.; Uchida, S.; Yeardley, D. J. P.; Ungar, G. *Biomacromolecules* **2001**, *2*, 729–740.

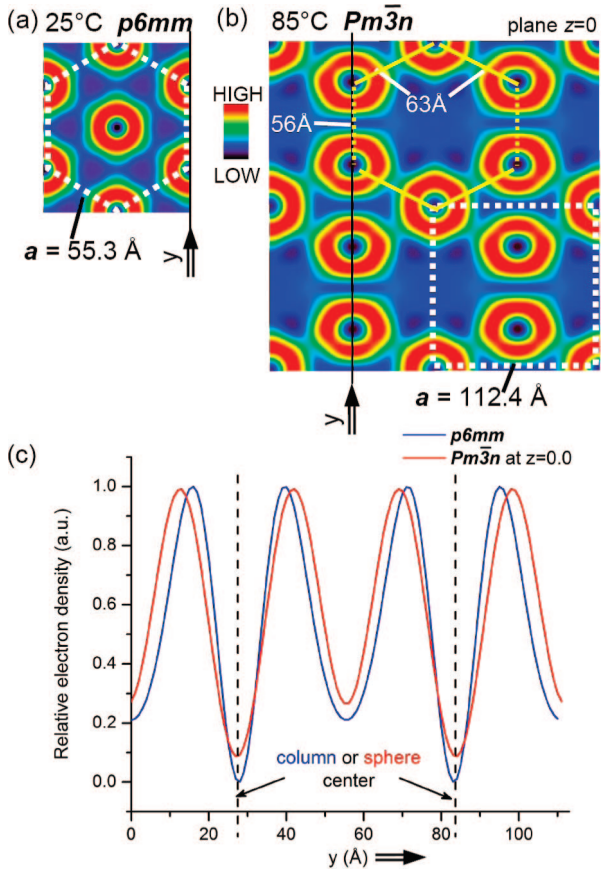

Figure 3. Reconstructed relative electron density maps of **7** in Φ_h (*p6mm*) and cubic (*Pm*$\bar{3}$*n*) phases: (a) *p6mm* phase at 25 °C; (b) *Pm*$\bar{3}$*n* cubic phase at 85 °C; (c) relative electron density profiles in *p6mm* and *Pm*$\bar{3}$*n* phases, plotted along the *y* direction. In panels a and b, double arrows indicate the *y*-direction used in the plots from panel c; in panel c, dashed lines indicate the positions of the column center (*p6mm* phase) or sphere center (*Pm*$\bar{3}$*n* phase).

An important structural event for the discussion that follows was provided by **7**. This dendron assembles at low temperature (Figure SF1c in Supporting Information; Table 1) in a porous column that self-organizes in a *p6mm* Φ_h lattice and at high temperature into a hollow sphere that self-organizes into a *Pm*$\bar{3}$*n* cubic lattice. Therefore this compound, together with the two constitutional isomers (4-3,4-3,5)12G2-CH_2-Boc-L-Tyr-L-Ala-OMe and (4-3,4-3,4)12G2-CH_2-Boc-L-Tyr-L-Ala-OMe, provides us with the opportunity to compare the structure of a porous column with that of a hollow sphere and to estimate the similarities between these structures by XRD and electron-density maps. DSC traces from Figure SF1 in Supporting Information and the data from Table 1 show a broad range of temperatures for all supramolecular assemblies, and this range allowed us to perform detailed XRD experiments as a function of temperature. In general, incorporation of chiral branches in the aliphatic chains of the dendrons eliminated the columnar assemblies and maintained only the spherical assemblies. Thermal transitions and their enthalpy changes are summarized in Table 1.

Screening for Hollow Spherical Supramolecular Dendrimers via Small-Angle Powder XRD. Since the intensity of higher-order diffraction peaks depends strongly on rapid variations of the electron density, we anticipate that enhanced amplitudes of the higher-order diffraction peaks of the *Pm*$\bar{3}$*n* cubic periodic array would indicate the potential of a hollow supramolecular sphere for structures with alkyl groups on their periphery, as was previously observed in a variety of porous columnar lattices.[13a] These enhanced amplitudes, when observed in structures generated from dendritic assemblies based on the same primary structure, are expected to be accompanied by an increase in the sphere diameter (D_{sphere}) and the lattice dimension (a) simultaneously with formation of a hollow core with diameter D_{core}. The increased amplitude of the higher-order reflections is mainly due to increased electron density contrast and, to a smaller extent, by the volume fractions of individual aliphatic and aromatic components of the structure. The minor role played by different volume fractions on the increased

(10) (a) Cho, B.-K.; Jain, A.; Gruner, S. M.; Wiesner, U. *Science* **2004**, *305*, 1598–1601. (b) Bury, I.; Heinrich, B.; Bourgogne, C.; Guillon, D.; Donnio, B. *Chem.—Eur. J.* **2006**, *12*, 8396–8413. (c) Cho, B.-K.; Jain, A.; Mahajan, S.; Ow, H.; Gruner, S. M.; Wiesner, U. J. *Am. Chem. Soc.* **2004**, *126*, 4070–4071. (d) Frauenrath, H. *Prog. Polym. Sci.* **2005**, *30*, 325–384. (e) Coco, S.; Cordovilla, C.; Donnio, B.; Espinet, P.; Garcia-Casas, M. J.; Guillon, D. *Chem.—Eur. J.* **2008**, *14*, 3544–3552. (f) Saez, I. M.; Goodby, J. W.; Richardson, R. M. *Chem.—Eur. J.* **2001**, *7*, 2758–2764. (g) Chung, Y.-W.; Lee, J.-K.; Zin, W.-C.; Cho, B.-K. *J. Am. Chem. Soc.* **2008**, *130*, 7139–7147. (h) Zeng, F.; Zimmerman, S. C. *Chem. Rev.* **1997**, *97*, 1681–1712. (i) Kim, H.-J.; Lee, E.; Kim, M. G.; Kim, M.-C.; Lee, M.; Sim, E. *Chem.—Eur. J.* **2008**, *14*, 3883–3888. (j) Ziherl, P.; Kamien, R. D. *Phys. Rev. Lett.* **2000**, *85*, 3528–3513. (k) Donnio, B; Buathong, S.; Bury, I.; Guillon, D. *Chem. Soc. Rev.* **2007**, *36*, 1495–1513. (l) Lenoble, J.; Campidelli, S.; Maringa, N.; Donnio, B.; Guillon, D.; Yevlampieva, N.; Deschenaux, R. *J. Am. Chem. Soc.* **2007**, *129*, 9941–9952. (m) Ungar, G.; Zeng, X. *Soft Matter* **2005**, *1*, 95–106. (n) Canilho, N.; Kasëmi, E.; Mezzenga, R.; Schlüter, A. D. *J. Am. Chem. Soc.* **2006**, *126*, 13998–13999. (o) Caminade, A.-M.; Turrin, C.-O.; Sutra, P.; Majoral, J.-P. *Curr. Opin. Colloid Interface Sci.* **2003**, *8*, 282–295. (p) Tschierske, C. *Curr. Opin. Colloid Interface Sci.* **2002**, *7*, 69–80. (q) Ponomarenko, S. A.; Boiko, N. I.; Shibaev, V. P. *Polym. Sci., Ser. C* **2001**, *43*, 1–45. (r) Suárez, M.; Lehn, J.-M.; Zimmerman, S. C.; Skoulios, A.; Heinrich, B. *J. Am. Chem. Soc.* **1998**, *120*, 9526–9532. (s) Diele, S. *Curr. Opin. Colloid Interface Sci.* **2002**, *7*, 333–342. (t) Baars, M. W. P. L.; Söntjens, S. H. M.; Fischer, H. M.; Peerlings, H. W. I.; Meijer, E. W. *Chem.—Eur. J.* **1998**, *4*, 2456–2466. (u) Matthews, O. A.; Shipway, A. N.; Stoddart, J. F. *Prog. Polym. Sci.* **1998**, *23*, 1–56.

(11) (a) Yeardley, D. J. P.; Ungar, G.; Percec, V.; Holerca, M. N.; Johansson, G. *J. Am. Chem. Soc.* **2000**, *122*, 1684–1689. (b) Duan, H.; Hudson, S. D.; Ungar, G.; Holerca, M. N.; Percec, V. *Chem.—Eur. J.* **2001**, *7*, 4134–4141. (c) Ungar, G.; Liu, Y. S.; Zeng, X. B.; Percec, V.; Cho, W. D. *Science* **2003**, *299*, 1208–1211. (d) Zeng, X. B.; Ungar, G.; Liu, Y. S.; Percec, V.; Dulcey, S. E.; Hobbs, J. K. *Nature* **2004**, *428*, 157–160.

(12) Rudick, J. G.; Percec, V. *Acc. Chem. Res.* **2008**, ASAP, 10.1021/ar800086w.

(13) (a) Percec, V.; Dulcey, A. E.; Balagurusamy, V. S. K.; Miura, Y.; Smidrkal, J.; Peterca, M.; Nummelin, S.; Edlund, U.; Hudson, S. D.; Heiney, P. A.; Hu, D. A.; Magonov, S. N.; Vinogradov, S. A. *Nature* **2004**, *430*, 764–768. (b) Percec, V.; Dulcey, A.; Peterca, M.; Ilies, M.; Miura, Y.; Edlund, U.; Heiney, P. A *Aust. J. Chem.* **2005**, *58*, 472–482. (c) Percec, V.; Dulcey, A. E.; Peterca, M.; Ilies, M.; Ladislaw, J.; Rosen, B. M.; Edlund, U.; Heiney, P. A. *Angew. Chem., Int. Ed.* **2005**, *44*, 6516–6521. (d) Percec, V.; Dulcey, A. E.; Peterca, M.; Ilies, M.; Sienkowska, M. J.; Heiney, P. A. *J. Am. Chem. Soc.* **2005**, *127*, 17902–17909. (e) Percec, V.; Dulcey, A. E.; Peterca, M.; Ilies, M.; Nummelin, S.; Sienkowska, M. J.; Heiney, P. A. *Proc. Natl. Acad. Sci. U.S.A.* **2006**, *103*, 2518–2523. (f) Peterca, M.; Percec, V.; Dulcey, A. E.; Nummelin, S.; Korey, S.; Ilies, M.; Heiney, P. A. *J. Am. Chem. Soc.* **2006**, *128*, 6713–6720. (g) Percec, V.; Dulcey, A. E.; Peterca, M.; Adelman, P.; Samant, R.; Balagurusamy, V. S. K.; Heiney, P. A. *J. Am. Chem. Soc.* **2007**, *129*, 5992–6002. (h) Percec, V.; Rudick, J. G.; Peterca, M.; Wagner, M.; Obata, M.; Mitchell, C. M.; Cho, W. D.; Balagurusamy, V. S. K.; Heiney, P. A. *J. Am. Chem. Soc.* **2005**, *127*, 15257–15264. (i) Percec, V.; Smidrkal, J.; Peterca, M.; Mitchell, C. M.; Nummelin, S.; Dulcey, A. E.; Sienkowska, M. J.; Heiney, P. A. *Chem.—Eur. J.* **2007**, *13*, 3989–4007. (j) Kaucher, M. S.; Peterca, M.; Dulcey, A. E.; Kim, A. J.; Vinogradov, S. A.; Hammer, D. A.; Heiney, P. A.; Percec, V. *J. Am. Chem. Soc.* **2007**, *129*, 11698–11699.

(14) Percec, V.; Won, B.; Peterca, M.; Heiney, P. A. *J. Am. Chem. Soc.* **2007**, *129*, 11265–11278.

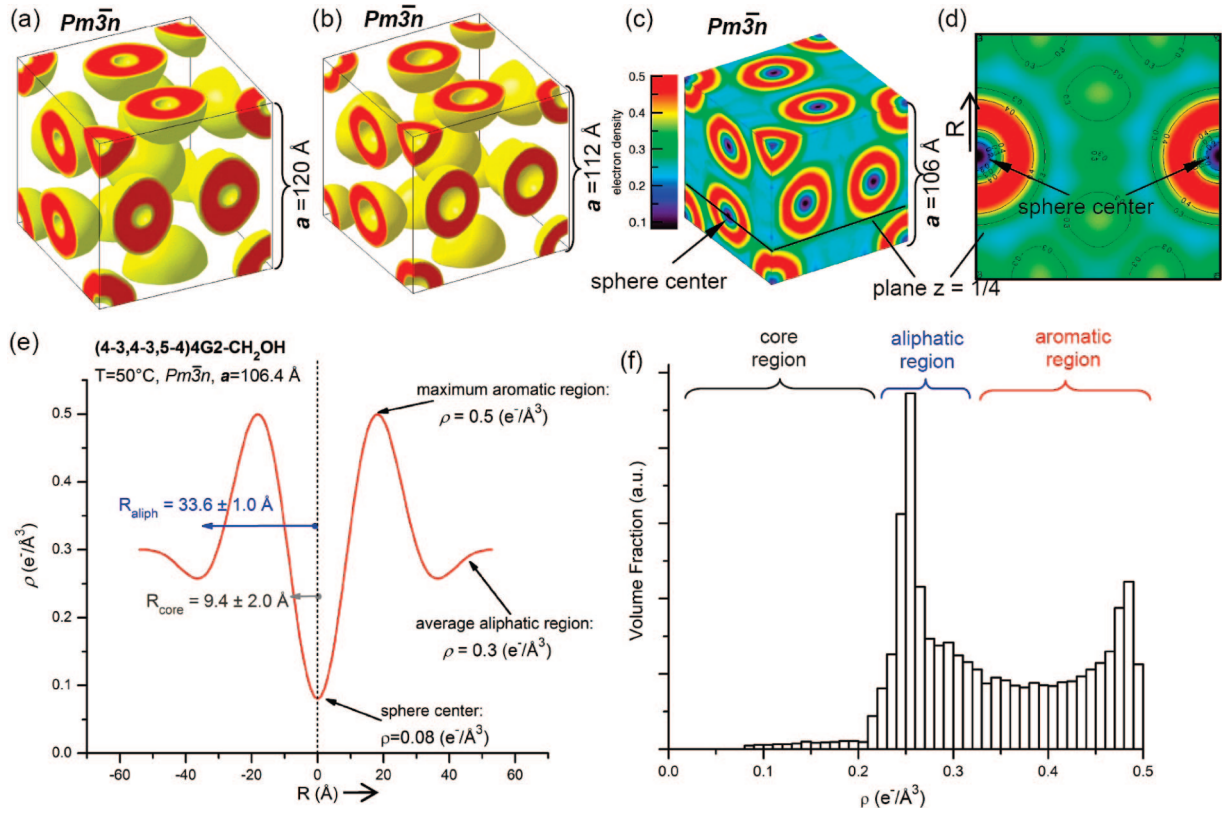

Figure 4. Reconstructed three-dimensional absolute electron density maps of the hollow cubic phases: (a) (4-3,4-3,5-4)12G2-CH_2OH (**8**), $Pm\bar{3}n$ phase; (b) (4-3,4-3,5-4)6G2-CH_2OH (**7**), $Pm\bar{3}n$ phase; (c) (4-3,4-3,5-4)4G2-CH_2OH (**6**), $Pm\bar{3}n$ phase. (d) Two-dimensional cross-section of the $z = {}^1/_4$ plane from panel c and (e) corresponding electron density profile; values assumed for the electron density of aliphatic and aromatic regions are shown together with the three-level fitted parameters. (f) Histogram of the volumetric electron density distribution from panel c, demonstrating the phase segregation model of the sphere. In panels a and b, only the high electron density regions are shown; in panel c, the full distribution is shown together with the color scale bar.

amplitude of higher-order reflections will be demonstrated in a separate publication. Figure 1 presents representative small-angle XRD for (4-3,4-3,4)12G2-X with X = CH_2-Boc-L-Tyr-L-Ala-OMe (**1**), CO_2CH_3 (**2**), and CH_2OH (**3**) (Figure 1a) together with an enlargement that allowed us to visualize the difference in peak relative amplitudes for the same library (Figure 1b). Lattice dimensions (a) and D_{core}, calculated by methods to be elaborated later, are also marked in Figure 1. The amplitude of the diffraction peaks and the values of a and D_{core} increase by changing X from CH_2OH (**3**) to CO_2CH_3 (**2**) and to CH_2-Boc-L-Tyr-L-Ala-OMe (**1**). This dependence was used to indicate the potential structure of a hollow spherical dendrimer.

The complete set of XRD results is available in Table 2. Figure 2a provides representative XRD data for (4-3,4-3,5-4)nG2-CH_2OH with n = 12 (**8**), 6 (**7**), and 4 (**6**) in the Φ_h and $Pm\bar{3}n$ cubic phases. A decrease in D_{core} as n increases from 4 to 12 is observed. At the same time, the decrease in D_{core} is accompanied by decreasing relative amplitude of higher-order peaks. This suggests that D_{core} increases with decreasing number of carbons from the tail length n, following the same trend as that observed for columnar phases.[13a] Amplitude in the Φ_h $p6mm$ phase correlates with amplitude in the $Pm\bar{3}n$ phase of the same molecule (Figure 2a,d). This suggests that most probably the mechanisms of pore and hollow core formation in supramolecular columns and spheres are related. This process will be described in a later subchapter. Figure 2b illustrates the XRD of (4-3,4-3,5-4^2)nG2-CH_2OH with n = 12 (**15**), 10 (**14**), 8 (**13**), 6 (**12**), and 4 (**11**). All compounds with n = 12−4 form $Pm\bar{3}n$ hollow assemblies. Finally, Figure 2c shows the XRD for **4**, **5**, **9**, and **10**, with X = CO_2CH_3 (**4** and **9**) and CH_2OH (**5** and **10**). Regardless of the structure of X, D_{sphere} increases at the transition from (4-3,4-3,4)dm8*G2-X (**4** and **5**) to (4-3,4-3,5-4)dm8*G2-X (**9** and **10**).

Reconstruction of Electron Density Maps. The electron density maps were reconstructed via principles previously employed for the supramolecular columns self-organized in the Φ_h phase[13a,f] and for spheres in the $Pm\bar{3}n$ phase.[5a] We assumed that the assembly process takes place by segregating the aromatic and aliphatic parts of the molecule in different regions, each with a constant electron density that can be calculated from the known atomic composition of that region.[5a,7a,c,11,12,13a,15] Figure 3 shows the reconstructed electron density maps of (4-3,4-3,5-4)6G2-CH_2OH (**7**) columns in the $p6mm$ Φ_h phase at 25 °C (panel a) and of the spheres in the $Pm\bar{3}n$ cubic phase at 85 °C (panel b). If we compare the cross section of the columns (Figure 3a) with the cross section of the spheres at the plane z = 0 (see the pseudohexagonal yellow marked arrangement), we observe a similar electron density in columns and in spheres. At the same time, we notice the resemblance between the column diameter and the sphere diameter (compare a in Figure 3a with yellow pseudohexagonal sites in Figure 3b). This shows that the spheres from the base plane of the $Pm\bar{3}n$ lattice that are in close contact (marked with dotted lines in the pseudohexagon) are similar in type and internal structure to the columns forming the hexagonal lattice. These results are expected when it is considered that the size of the $Pm\bar{3}n$ cubic lattice (a = 112.4 Å, Figure 3b) is double the size of the hexagonal lattice

(15) Ungar, G.; Abramic, D.; Percec, V.; Heck, J. A. *Liq. Cryst.* **1996**, *21*, 73–86.

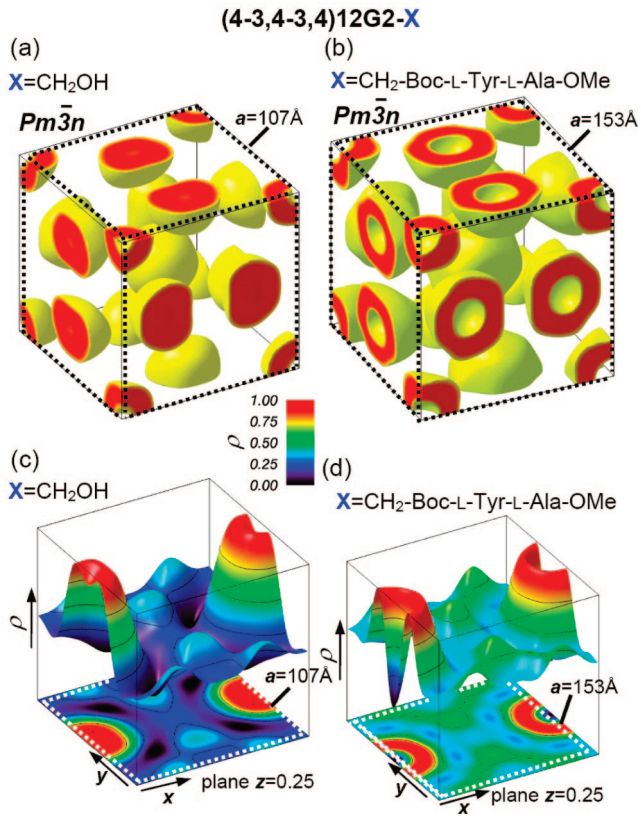

Figure 5. Reconstructed relative three-dimensional (a, b) and two-dimensional cross sections (c, d) of relative electron densities of (4-3,4-3,4)12G2-X in the $Pm\bar{3}n$ phase. In panels a and b, only the high electron density regions are shown. The lattice unit cell is indicated by dotted lines. Lattice parameter a, z-plane positions, and X are indicated.

(a = 55.3 Å, Figure 3a). Figure 3c shows the relative electron density profiles of the $p6mm$ and $Pm\bar{3}n$ lattices along the y direction. The black dotted line indicates the position of the column center (blue) for the hexagonal $p6mm$ phase or sphere center (red). This plot also illustrates that both supramolecular structures have a low density at their core that is not zero due to the presence of transient guest molecules; therefore, they are hollow. The similarity between the electron densities and sizes of the columns and spheres from Figure 3 guarantees application of the same assembly and electron density reconstruction principles both for porous columns and for hollow spheres.

These results allowed us to reconstruct absolute 3-D electron density maps for the hollow spheres self-organized in a $Pm\bar{3}n$ cubic phase (Figure 4). For simplicity in Figure 4a,b only the high electron density is shown for the hollow spheres with small and large D_{core} generated from (4-3,4-3,5-4)nG2-CH_2OH with n = 12 (**8**) (Figure 4a) and n = 6 (**7**) (Figure 4b) in the $Pm\bar{3}n$ lattice. Hollow spheres are observed in both cases. However, as predicted by the amplitudes of the XRD data from Figure 2a, although D_{col} of **8** is larger than for **7**, the hollow core of **7** is larger (Scheme 1). This trend can be attributed to a reduced distribution of gauche conformers in the alkyl groups that increases inter- or intramolecular interactions when the alkyl chain length is reduced. At the same time, by reducing the thickness of the aliphatic region of the supramolecular assemblies, the relative amplitudes of the diffraction peak can be enhanced due to increased contrast between the average electron density of aliphatic and aromatic regions.

The reconstructed absolute electron density of the supramolecular spheres assembled from (4-3,4-3,5-4)4G2-CH_2OH (**6**) is shown in Figure 4c. The absolute electron density distribution from Figure 4c−e was calculated from the reconstructed relative electron density. With the assumption that the average electron density (ρ) of the aliphatic region is 0.3 $e^-/Å^3$[16] and the maximum electron density in the aromatic region is 0.5 $e^-/Å^3$,[16] the relative electron density was converted to the absolute electron density following a linear transformation. The values of the electron densities were selected from literature compounds with related structures,[16] and work to be reported elsewhere confirms that these density values are accurate. The resulting absolute electron density for the $Pm\bar{3}n$ phase self-assembled from **6** (Figure 4e) shows that at the center of the supramolecular spheres the electron density is lower than 0.08 $e^-/Å^3$. This result demonstrates that the core region is at least 4 times less dense than the aliphatic region from the periphery of the sphere. It has to be mentioned that the electron density region at the center of the sphere can be slightly lower or higher when more Fourier components are included. The data shown in Figure 4 were reconstructed on the basis of a finite number of Fourier components given by the first 20 diffraction peaks of the $Pm\bar{3}n$ phase. Additional higher-order diffraction peaks ($h \geq 4$, Supporting Information) were experimentally observed, but due to their overlap, no accurate deconvolution was possible.

The phase segregation model advanced for the supramolecular spheres[5a] was demonstrated by the histogram shown in Figure 4f. The two maxima in the volume fraction correspond to segregation of the aromatic and aliphatic regions, respectively. The histogram for the empty core region is uniform and indicates that it extends in a relatively small fraction of the unit cell.

The high 3-D relative electron density regions of the $Pm\bar{3}n$ lattice of (4-3,4-3,4)12G2-X with X = CH_2OH (**3**) and X = CH_2-Boc-L-Tyr-L-Ala-OMe (**1**) are shown in Figure 5a,b. The transition from a sphere with a very small or no hollow center to a sphere with a large hollow center is generated by addition of the dipeptide at the apex of dendron **3**. The 2-D cross section of the relative electron density at plane z = 0.25 for dendritic dipeptide **1** assemblies is shown in Figure 5d, while that for dendron **3** is shown in Figure 5c. Due to H-bonding, in the case of the sphere with X = CH_2OH (**3**) at the dendron apex a very small or no hollow core is observed (Figure 5a). The replacement of X = CH_2OH with X = CO_2CH_3 (**2**) releases the contraction induced by H-bonding and allows the formation of a hollow center in the self-assembled supramolecular spheres (Table 3, Figure 1).

We must clarify at this point the meaning of a hollow supramolecular dendrimer. By analogy with spherical hollow proteins that are widespread in biological systems,[17,18] they are globular or icosahedral structures that exhibit a spherical hollow shell or cagelike shape with an interior space. There is no vacuum in this interior space. Hydrophobic protein cavities contain water molecules with subnanosecond residence times. Polar protein cavities tend to be occupied by structural water molecules. Hydrophobic pores[13a,j] are populated by water molecules with very short residence times. Therefore, by analogy with biological proteins, the cavity of the hollow supramolecular spherical dendrimers must contain either water or other transient

(16) Turner, D. C.; Gruner, S. M. *Biochemistry* **1992**, *31*, 1340–1355.
(17) (a) Qvist, J.; Davidovic, M; Hamelberg, D.; Halle, B. *Proc. Natl. Acad. Sci. U.S.A.* **2008**, *105*, 6296–6301. (b) Banyard, S. H.; Stammers, D. K.; Harrison, P. M. *Nature* **1978**, *271*, 282–284. (c) Sano, K.-I.; Ajima, K.; Iwahori, K.; Yudasaka, M.; Iijima, S.; Yamashita, I.; Shiba, K. *Small* **2005**, *1*, 826–832.
(18) (a) Klug, A. *Angew. Chem., Int. Ed. Engl.* **1983**, *22*, 565–582. (b) Klug, A. *Philos. Trans. R. Soc. London, Ser. B* **1999**, *354*, 531–535.

Table 3. Structural and Retrostructural Analysis of the Dendritic and Dendritic Dipeptide Library That Self-Assemble into Porous Columns or Hollow Spheres

dendron	T (°C)	phase	a^a (Å)	R_{core} (Å); R_{aliph} (Å); α, β^b	D_{sphere} measured/fitted (Å)	ρ (g/cm^3)	μ^c	D_{core} or D_{pore} (Å)
(4-3,4-3,4)12G2-CO_2CH_3 **2**	150	$Pm\bar{3}n$	118.5	8.3	73.5^d/74.5^e	1.05 ^{f}	87	16.6 ± 4.0^e
				37.2	59.2^g/59.5^h			13.3 ± 3.5^h
				0.799, 0.888	67.2^i/66.2^j			14.7 ± 4.0^j
(4-3,4-3,4)dm8*G2-CO_2CH_3 **4**	140	$Pm\bar{3}n$	108.8	8.2	67.5^d/67.7^e	1.056	73	16.4 ± 4.0^e
				33.8	54.4^g/54.4^h			13.2 ± 3.5^h
				0.805, 0.894	60.8^i/60.5^j			14.6 ± 4.0^j
(4-3,4-3,4)12G2-CH_2-Boc-L-Tyr-L-Ala-OMe **1**	140	$Pm\bar{3}n$	153	10.0	94.9^d/95.0^e	1.055	155	20.0 ± 4.0^e
				47.5	76.5^g/75.4^h			15.9 ± 3.5^h
				0.794, 0.873	85.5^i/82.9^j			17.4 ± 4.0 ^{j}
(4-3,4-3,5-4)4G2-CH_2OH **6**	50	$Pm\bar{3}n$	106.4	9.4	66.0^d/67.2^e	0.99 ^{f}	72	18.8 ± 4.0^e
				33.6	53.2^g/53.5^h			14.9 ± 3.5^h
				0.797, 0.906	59.5^i/60.8^j			17.0 ± 4.0^j
(4-3,4-3,5-4)6G2-CH_2OH **7**	25	*p6mm*	55.3		27.6/26.0 ^{k}	0.974	6	11.2 ± 1.6^f
	90	$Pm\bar{3}n$	112.4	8.3	69.7^d/72.2^e		83	16.6 ± 4.0^e
				36.1	56.2^g/56.2^h			12.9 ± 3.5^h
				0.778, 0.878	62.8^i/63.4 ^{j}			14.6 ± 4.0^j
(4-3,4-3,5-4)dm8*G2-CO_2CH_3 **9**	50	$Pm\bar{3}n$	120.0	10.9	74.4^d/72.8^e	1.05^f	91	21.8 ± 4.0^e
				36.4	60.0^g/58.5^h			17.5 ± 3.5^h
				0.803, 0.876	67.1^i/63.7^j			19.1 ± 4.0^j
(4-3,4-3,5-4)dm8*G2-CH_2OH **10**	65	$Pm\bar{3}n$	117.4	8.8	72.6^d/70.8^e	1.06 ^{f}	87	17.6 ± 4.0^e
				35.4	58.5^g/57.3^h			14.2 ± 3.5^h
				0.809, 0.905	65.4^i/64.1^j			15.9 ± 4.0^j
(4-3,4-3,5-4^2)4G2-CH_2OH **11**	55	$Pm\bar{3}n$	132.5	13.2	82.2^d/79.6^e	1.1 ^{f}	155	26.4 ± 4.0^e
				39.8	66.3^g/66.4^h			22.0 ± 3.5^h
				0.834, 0.943	74.1^i/75.0^j			24.9 ± 4.0^j
(4-3,4-3,5-4^2)6G2-CH_2OH **12**	80	$Pm\bar{3}n$	134.7	12.9	83.5^d/82.2^e	1.1 ^{f}	149	25.8 ± 4.0^e
				41.1	67.4^g/67.3^h			21.1 ± 3.5^h
				0.819, 0.918	75.3^i/75.5^j			23.6 ± 4.0^j
(4-3,4-3,5-4^2)8G2-CH_2OH **13**	95	$Pm\bar{3}n$	137	11.6	84.9^d/87.4^e	1.09 ^{f}	143	23.2 ± 4.0^e
				43.7	68.5^g/68.3^h			18.1 ± 3.5^h
				0.782, 0.904	76.6^i/79.0^j			20.9 ± 4.0^j
(4-3,4-3,5-4^2)10G2-CH_2OH **14**	100	$Pm\bar{3}n$	138	10.6	85.6^d/87.8^e	1.07 ^{f}	132	21.2 ± 4.0^e
				43.9	69.0^g/70.9^h			17.1 ± 3.5^h
				0.808, 0.908	77.1^i/79.7^j			19.2 ± 4.0^j
(4-3,4-3,5-4^2)12G2-CH_2OH **15**	110	$Pm\bar{3}n$	139	10.3	86.2^d/87.8^e	1.053	126	20.6 ± 4.0^e
				43.2	69.5^g/70.9^h			16.9 ± 3.5^h
				0.825, 0.913	77.7^i/79.7^j			18.8 ± 4.0^j

^{a} Lattice parameter. ^{b} The first entry for each dendron is R_{core}, the second entry is R_{aliph}, and the third entry gives three-level fitted parameters α and β. ^{c} Number of dendrons per spherical cluster, calculated from $\mu_{Pm\bar{3}n} = \rho a^3 N_A/(8M_{wt})$, and per column stratum, calculated from $\mu_{p6mm} = \rho\sqrt{3}a^2 t N_A/(2M_{wt})$ where ρ = density at 20 °C, t = average column stratum thickness; $N_A = 6.022 \times 10^{23}$ mol^{-1} = Avogadro's number, and M_{wt}= molecular weight. ^{d} Spherical cluster diameter was calculated from $D_{sphere} = 2a/(32\pi/3)^{1/3}$, which divides the unit cell volume into eight identical spheres. ^{e} Type II (face) sphere or core diameters along the direction perpendicular to their close contact were calculated from $D_{sphere} = 2R_{aliph}$ or $D_{core} = 2R_{core}$. ^{f} Estimated density. ^{g} Spherical cluster diameter was calculated from $D_{sphere} = a/2$, which gives directly the diameter along the close contact of the face "spherical" clusters. ^{h} Type II (face) sphere or empty core diameters along the direction of their close contact were calculated from $D_{sphere} = 2\alpha R_{aliph}$ or $D_{core} = 2\alpha R_{core}$. ^{i} Spherical cluster diameter was calculated from $D_{sphere} = \sqrt{(a/2)^2 + (a/4)^2}$, which gives the distance between the center of the face cluster and the center of the close-by corner cluster ^{j} Type I (corner/center) sphere or empty core diameters were calculated from $D_{sphere} = 2\beta R_{aliph}$ or $D_{core} = 2\beta R_{core}$. ^{k} Column or pore diameter was calculated from the three-level fit for the columnar phases.[13f]

guests that cannot be detected at the resolution of the current XRD and TEM experiments. The transient guests can be replaced by other species. Experiments on this line will be reported later.

Imaging by TEM Combined with Electron Diffraction Experiments. Low-dose ED and TEM images of a quenched single-crystal sample (from approximately 130 °C) of **1** were obtained at cryogenic temperature (Figure 6a). In both ED and TEM imaging, from large single-crystal domains, observations were made of the [012] and [001] zones. The [012] zone axis is normal to the plane, indicating that a plane of type (210) is in contact with the substrate. While the areal density of quasi-spherical aggregates of this plane is slightly less than that of the (200), the intensity of the (210) reflection is significantly greater than that of (200). This greater intensity for the (210), a characteristic of these hollow spheres assembled in the $Pm\bar{3}n$ lattice, manifests planes that are more sharply defined from the (200). These factors such as high areal density, usually associated with low-index planes, and sharply defined planes help to determine the preferred contact plane. In this zone, six unique Fourier components were observed. The [001] zone axis was observed by tilting 26° about the [100], and 11 unique components were observed. The defocus of the image in Figure 6a is approximately −1200 nm, so that the resolution limit (as measured by the first zero in the contrast transfer function, CTF) is 1.9 nm, that is, less than $^1/_7$ of the cubic lattice parameter. All of the Fourier components captured in this image thus fall within the first envelope of the CTF. A remarkable feature of the TEM image (Figure 6a) is the appearance of circular features arranged on a square lattice. The TEM image is a projection through the periodic lattice, comprising quasi-spherical aggregates of **1**, in which dark regions correspond to relatively dense projections through the lattice. The light portion in the center of the circles indicates, therefore, that the aggregates are hollow, most probably as a core shell. In Figure 6b we compare the relative electron density maps of (4-3,4-3,4)12G2-CH_2-Boc-L-Tyr-L-Ala-OMe (**1**) at plane $z = 0$ of the $Pm\bar{3}n$ phase with the cross-section plane of the *p6mm* Φ_h phase of the porous (4-3,4-3,5)12G2-CH_2-Boc-L-

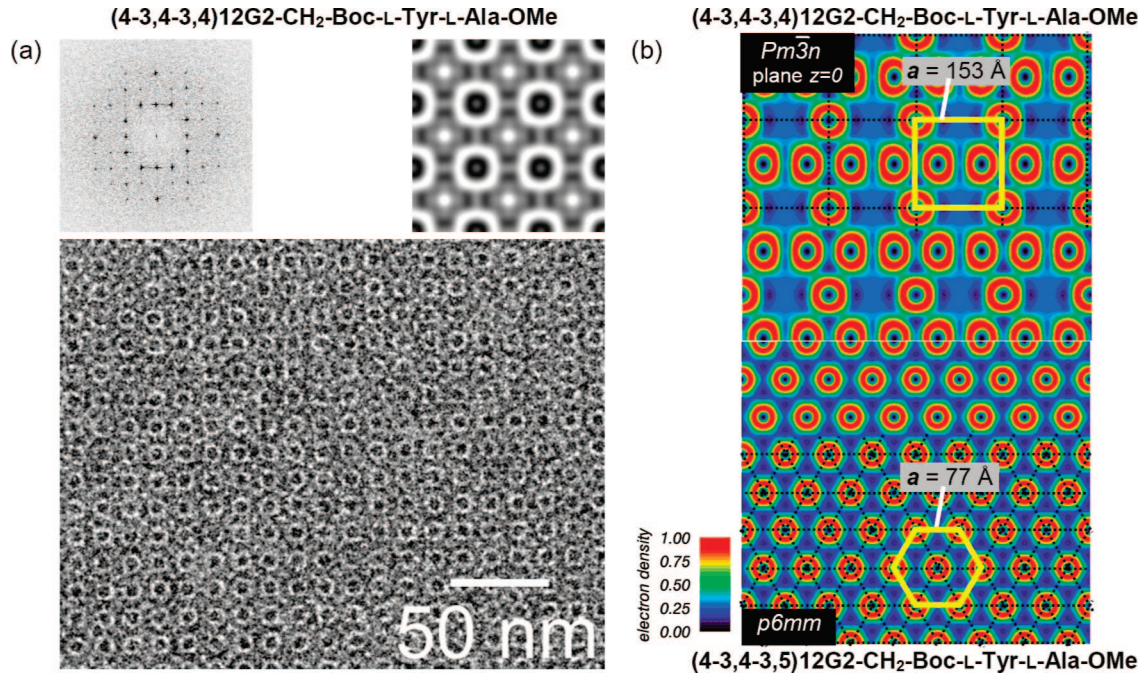

Figure 6. (a) TEM image and Fourier analysis of **1**. (Bottom) Raw TEM image; (upper right) Fourier transform of the TEM image; (upper left) corresponding image reconstruction from the Fourier transform. (b) Comparison of the relative electron density maps, presented on the same scale, of (top) (4-3,4-3,4)12G_2-CH_2-Boc-L-Tyr-L-Ala-OMe (**1**) in the *Pm*$\bar{3}$*n* cubic phase and (bottom) constitutional isomeric (4-3,4-3,5)12G_2-CH_2-Boc-L-Tyr-L-Ala-OMe[13a] in the *p6mm* porous hexagonal columnar phase, showing the similarity between hollow spheres and porous columns and between their lattice dimensions.

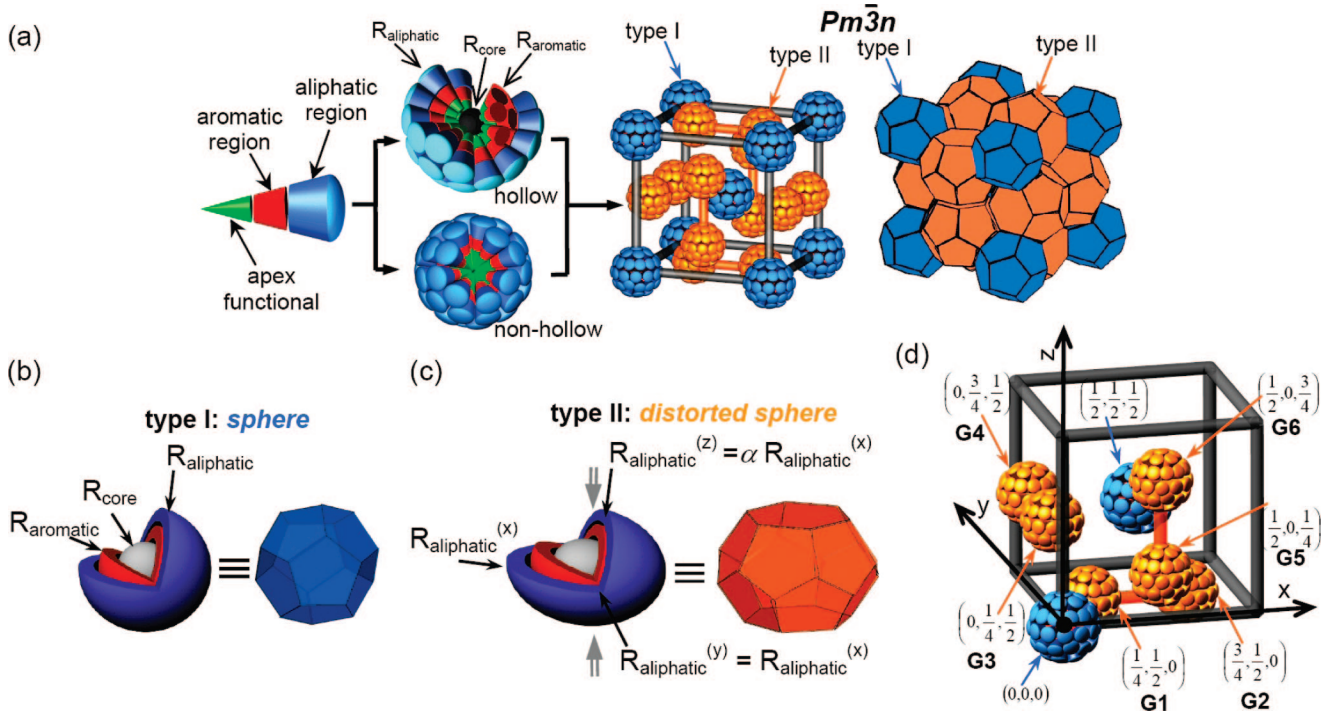

Figure 7. Three levels of constant electron density are used to model spherical supramolecular assemblies. (a) Schematic of *Pm*$\bar{3}$*n* cubic assembly and polyhedron space-filling view of the unit cell. (b, c) Simplified models of (b) spherical and (c) distorted spherical assemblies. (d) Normalized positions of the eight spherical objects that form the *Pm*$\bar{3}$*n* unit cell. Color code: core region, gray; aromatic region, red; aliphatic region, blue.

Tyr-L-Ala-OMe reported previously.[13a] The similarity between the dimensions and the structure of these spheres is as strong as in the case discussed in Figure 3.

Calculation of Dimensions of the Hollow Core of Supramolecular Spheres in the *Pm*$\bar{3}$*n* Cubic Assembly by Reconstruction of X-ray Diffraction. This calculation was accomplished by reconstruction of the XRD via a least-squares fit of the observed positions and amplitudes of the diffraction peaks to those calculated for a simplified model consisting of spherical or distorted spherical hollow shells or clusters of dendrons. Each spherical cluster consists of three concentric shells, each of constant electron density. The relative electron density in each shell is calculated from the molecular structure of the self-assembling dendron, and therefore, the only fitting

Table 4. S_{hkl}[a] Summations of Type I, Type II, and All Spherical Assemblies in the Case of the $Pm\bar{3}n$ Lattice

(*hkl*)	type I	type II	S_{hkl}	(*hkl*)	type I	type II	S_{hkl}
(110)	2	−2	0	(411)	2	−2	0
(200)	2	2	4	(330)	2	−2	0
(210)	**0**	**4**	**4**[b]	(420)	2	2	4
(211)	2	2	4	**(421)**	**0**	**4**	**4**[b]
(220)	2	−2	0	(332)	2	2	4
(310)	2	−2	0	(422)	2	−2	0
(222)	2	−6	−4	(430)	0	0	0
(320)	**0**	**−4**	**-4**[b]	(431)	2	−2	0
(321)	2	2	4	**(432)**	**0**	**−4**	**−4**[b]
(400)	2	6	8	(440)	2	6	8
(410)	0	0	0	(442)	2	2	4

[a] The listed values correspond to the case when the type I is identical with the type II assembly (Figure 7a) [b] Prefactors shown in boldface type change sign when the other orientation for the unit cell is chosen, that is, a 90° rotation along the *z*-axis for the choice shown in Figure 7d (for details see Figure SF5 in Supporting Information).

parameters are the shell radii. Similar principles were previously used to reconstruct the lyotropic hexagonal phase generated from lipids[16] and the circular[13a] and elliptical[13f] porous hexagonal and rectangular phases of self-assembling dendrons. Schematic representations of the three-level model of supramolecular spherical or distorted hollow spherical clusters that self-assemble in the $Pm\bar{3}n$ cubic lattice are illustrated in Figure 7.

The scattering amplitude from a cluster is given by the Fourier transform of the electron density, which for a solid sphere of constant density ($\rho = \rho_0$ for $r \leq R$, $\rho = 0$ for $r > R$) is given by eq 1:

$$F(\vec{q}) = \int \rho(\vec{r}) e^{i\vec{q}\,\vec{r}}\, d\vec{r} = \frac{\rho_0}{q^3}[\sin(qR) - qR\cos(qR)] \equiv F_{sp}(q, R, \rho_0) \quad (1)$$

The structure factor for three concentric spherical shells is given by eq 2:

$$F_{shell}(q) = F_{sp}(q, R_{al}, \rho_{al}) - F_{sp}(q, R_{ar}, \rho_{al}) + F_{sp}(q, R_{ar}, \rho_{ar}) - F_{sp}(q, R_c, \rho_{ar}) + F_{sp}(q, R_c, \rho_c) \quad (2)$$

where $\rho_{al} = 3N_{aliphatic}/[4\pi(R_{al}^3 - R_{ar}^3)]$, $N_{aliphatic}$ and $R_{aliphatic}$ [$=R_{al}$] are the number of electrons and radius for the aliphatic region, $\rho_{ar} = 3N_{aromatic}/[4\pi(R_{ar}^3 - R_c^3)]$, $N_{aromatic}$ and $R_{aromatic}$

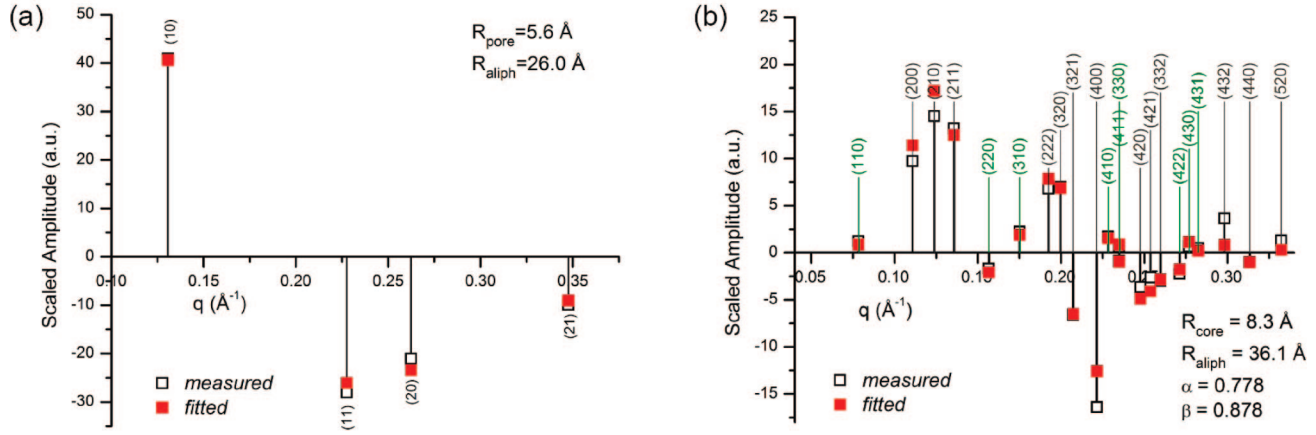

Figure 8. Comparison of the measured amplitudes (open squares) and three-level model fitted amplitudes (solid red squares) of **7** in (a) *p6mm* columnar hexagonal phase and (b) $Pm\bar{3}n$ cubic phase. The empty core diameter for $Pm\bar{3}n$ cubic phase along the close contact direction of the face spheres is $2\alpha R_{core} = 12.9 \pm 3.5$ Å, comparable to the pore diameter calculated for the hexagonal columnar phase $D_{pore} = 11.2 \pm 1.6$ Å. In panel b, the peaks marked in green have nonzero intensity only if type I and type II clusters are different from each other.

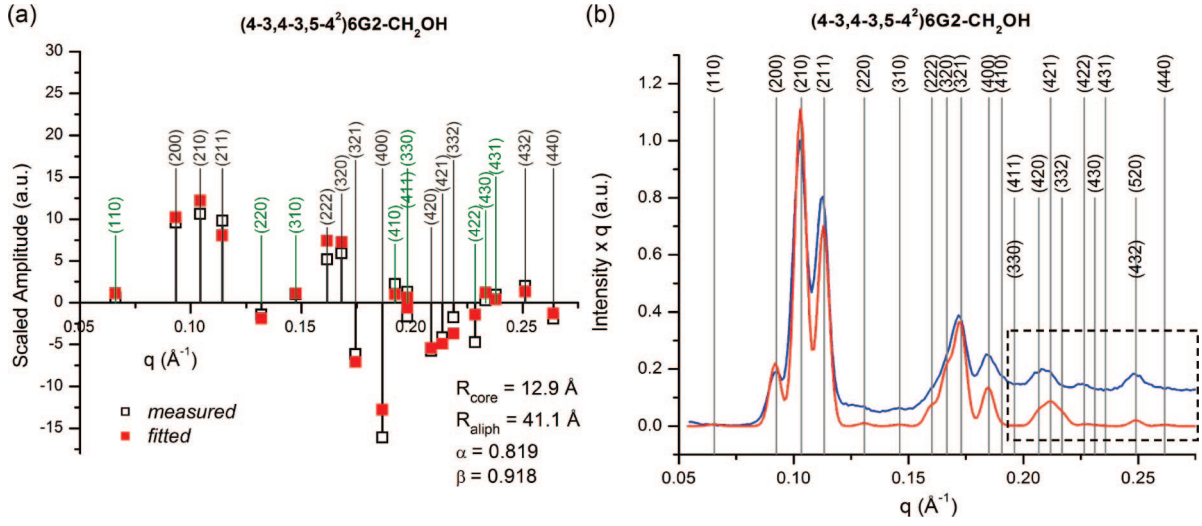

Figure 9. Comparison of (a) measured amplitudes (open squares) with three-level model fitted amplitudes (solid red squares) and of (b) measured (blue line) with fitted (red line) XRD peak amplitudes for the $Pm\bar{3}n$ lattice self-organized from the hollow supramolecular spheres self-assembled from (4-3,4-3,5-4^2)6G2-CH_2OH (**12**). In panel b, the dotted rectangle marks the region of higher-order peaks overlapping that starts with $q_{(hkl)} > q_{(330)}$. In the experimental plot, no background correction was applied.

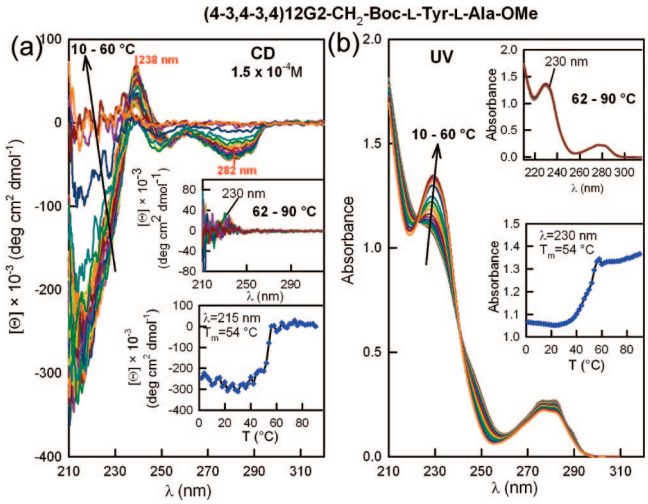

Figure 10. Temperature dependence of (a) CD and (b) UV spectra of **1** in methyl cyclohexane (1.5×10^{-4} M). Arrows indicate trends upon increasing temperature. (Lower insets) Changes in molecular ellipticity and absorbance as a function of temperature. (Upper insets) Cotton effect associated with molecular solution of the dendron.

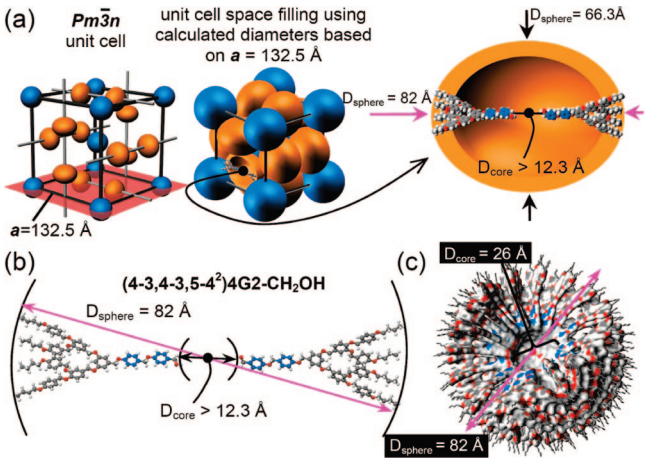

Figure 11. Molecular model of **11** in the $Pm\bar{3}n$ phase. (a, b) A dendron unit pair with its aliphatic chains in all-trans conformation provides the lower bound for D_{core}. (c) Spherical supramolecular assembly with a surface added to the aromatic region.

[$=R_{ar}$] are the number of electrons and radius for the aromatic region, $\rho_c = 3N_{core}/(4\pi R_c^3)$, and N_{core} and R_{core} [$=R_c$] are the number of electrons and radius for the core region (Figure 7a). The scattered amplitude is then given by eq 3:

$$A(q_{h,k,l}) = A_0 \sum_n e^{2\pi i(X_n h + Y_n k + Z_n l)} F_{shell,n}(q_{h,k,l}) \quad \text{where} \quad q_{h,k,l} = \frac{2\pi}{a}\sqrt{h^2+k^2+l^2} \quad (3)$$

In eq 3, A_0 is an arbitrary scale factor, $F_{shell,n}(q_{hkl})$ is the form factor for the nth sphere, a is the lattice parameter, and the summation is over all the spherical assemblies in the unit cell. The unit cell normalized values for (X_n, Y_n, Z_n) triplets in the case of the $Pm\bar{3}n$ cubic lattice are shown in Figure 7d. When all the spheres are identical, eq 3 reduces to eq 4:

$$A(q_{h,k,l}) = A_0 F_{shell}(q_{h,k,l}) S_{hkl} \quad \text{where} \quad S_{hkl} \equiv \sum_n e^{2\pi i(X_n h + Y_n k + Z_n l)} \quad (4)$$

Table 4 lists the calculated summations over type I, type II, and all other spherical assemblies shown in Figure 7a.

Experimental observation of (110), (220), (310) and (422) peaks with nonzero intensities indicates that the type I and II supramolecular assemblies cannot be identical, otherwise S_{hkl} would be zero for these peaks (Table 4). Moreover, the presence in the experimental data of a weak (410) peak (Figure SF2 in Supporting Information) implies that the form factors of at least one of the two types of supramolecular assemblies must vary, presumably by having a position-dependent orientational variation consistent with the lattice symmetry. In accordance with the observation that the type II assemblies from the faces of the lattice (Figure 7d) are in close contact, it is reasonable to allow type I and II assemblies to have different radii. If the type I and II spheres have locally the same electron density but different radii, they must have a different total number of electrons. In other words, the proposed parametrization accounts for the possibility of a different total number of dendrons for type I and II spherical assemblies. It was assumed that all three spherical radii are scaled by the same factor β defined in eq 5:

$$\beta = \frac{R_{al}^{\text{type I}}}{R_{al}^{\text{type II}}} = \frac{R_{ar}^{\text{type I}}}{R_{ar}^{\text{type II}}} = \frac{R_c^{\text{type I}}}{R_c^{\text{type II}}} \quad (5)$$

The deviation of type II assembly from spherical symmetry[5a] was modeled by assuming that each sphere was distorted by a factor α along the axis of close contact (Figure 7c). For example, a type II assembly positioned at ($^1/_2$, 0, $^1/_4$), (Figure 7d), assumed to have a constant electron density ρ_0 and to be distorted along the z axis (Figure 7c), has the spatial electron density distribution $\rho(x, y, z)$ given by eq 6:

$$\rho(x,y,z) = \begin{cases} \rho_0 & \text{if } \left(\frac{x}{R}\right)^2 + \left(\frac{y}{R}\right)^2 + \left(\frac{z}{\alpha R}\right)^2 \le 1 \\ 0 & \text{if } \left(\frac{x}{R}\right)^2 + \left(\frac{y}{R}\right)^2 + \left(\frac{z}{\alpha R}\right)^2 > 1 \end{cases} \quad (6)$$

The Fourier transform of the distribution from eq 6 was calculated with the changes of variables $x' = x$, $y' = y$, $z' = z/\alpha$, $q_x' = q_x$, $q_y' = q_y$, and $qz' = \alpha q_z$. This provides eq 7, in which q' is given by eq 8:

$$F_{\text{distorted-along-}z\text{-axis}}(\vec{q}) = \int \rho(\vec{r}) e^{i\vec{q}\,\vec{r}}\, d\vec{r} = \alpha F_{sp}(q', R, \rho_0) \quad (7)$$

$$q' = \sqrt{q_x^2 + q_y^2 + (\alpha q_z)^2} \quad (8)$$

Subsequently, these elements were combined to arrive at the scattered amplitude of the (hkl) diffraction peak of the $Pm\bar{3}n$ phase given by eq 9:

$$A(q_{h,k,l}) = A_0[S_I(q_{h,k,l}) + S_{II}(q_{h,k,l})] \quad (9)$$

In eq 9 the structure factor for the type I assembly is given by eq 10, in which $F_{cluster}(q, \beta)$ is given by eq 11:

$$S_I(q_{h,k,l}) = F_{cluster}(q_{h,k,l}, \beta)\{1 + \cos[\pi(h+k+l)]\} \quad (10)$$

$$F_{cluster}(q,\beta) \equiv F_{sp}(q, \beta R_{al}, \rho_{al}) - F_{sp}(q, \beta R_{ar}, \rho_{al}) + F_{sp}(q, \beta R_{ar}, \rho_{ar}) - F_{sp}(q, \beta R_c, \rho_{ar}) + F_{sp}(q, \beta R_c, \rho_c) \quad (11)$$

The form factors for type II assemblies from eq 9 depend on their orientation; consequently, the structure factor can be written as a cyclic permutation given by eq 12, in which G is defined in eq 13 and Q_{mnp} is defined in eq 14:

$$S_{II}(q_{h,k,l}) = G(h,k,l) + G(l,h,k) + G(k,l,h) \quad (12)$$

$$G(m,n,p) = \left\{\cos\left[2\pi\left(\frac{m}{4}+\frac{n}{2}\right)\right] + \cos\left[2\pi\left(\frac{3m}{4}+\frac{n}{2}\right)\right]\right\}\alpha F_{cluster}(Q_{mnp}, 1) \quad (13)$$

$$Q_{mnp} = \frac{2\pi}{a}\sqrt{(\alpha m)^2 + n^2 + p^2} \quad (14)$$

By use of measured XRD, amplitudes were fitted by varying the model parameters A, R_{al}, R_{ar}, and R_c and neither, one, or both of the α and β parameters for the $Pm\bar{3}n$ lattice by using eq 9. The intense (200), (210), and (211) peaks could not be adequately fit without varying the parameter α. In other words, the fit that considered that type I and II assemblies are identical spheres ($\alpha = \beta = 1$; Figure SF4a in Supporting Information) or that type I and II assemblies are spheres with different number of dendrons ($\alpha = 1$ fixed and β allowed to vary; Figure SF4b in Supporting Information) could not properly fit the amplitudes of these three most intense diffraction peaks. As expected, the addition of one or two more fitting parameters increases the error bars on the structural parameters obtained, compared to the three-level fits of the *p6mm* lattice. In general, the fit to the $Pm\bar{3}n$ phase could be further improved by varying β (Figure SF4 in Supporting Information). In all cases the parameter β was fitted to a value less than 1, indicating that assemblies from the faces of the lattice have, most probably, a larger number of dendrons per sphere than corner or center ones.

For all the reported results, the intensities of the diffraction peaks were also fitted, by simply squaring eq 9 for the $Pm\bar{3}n$ lattice. This test proved the validity of the results, since the intensity fit is independent of the peak amplitude phase choice. Within the method error, similar results were obtained from the two-level model that considers the aliphatic region to be approximated by a continuum aliphatic "sea". The two-level fits were based on eqs 9−14, with eq 11 replaced by eq 15:

$$F_{cluster}(q,\beta) \equiv F_{sp}(q, \beta R_{ar}, \rho_{ar} - \rho_{al}) - F_{sp}(q, \beta R_c, \rho_{ar}) + F_{sp}(q, \beta R_c, \rho_c) \quad (15)$$

Reconstruction of the amplitude and position of the XRD peaks of the *p6mm* porous columnar hexagonal assembly generated from **7**, following the previously elaborated method,[13a] is shown in Figure 8a. Reconstruction of the XRD for the hollow spherical $Pm\bar{3}n$ assembly generated by **7**, based on eq 9, is presented in Figure 8b. The data from Figure 8a provide $D_{pore} = 11.2 \pm 1.6$ Å, while the hollow spherical objects assembling into the $Pm\bar{3}n$ lattice from Figure 8b have $D_{core} = 12.9 \pm 3.5$ Å. The similar values were used to report the assembly mechanism discussed previously by the electron density maps of the same two structures (Figure 3). Figure 9 illustrates the quality of the XRD reconstruction via direct comparison of the scaled amplitudes (Figure 9a) or of the measured powder XRD plot with the reconstructed one (Figure 9b). D_{core} values for all hollow spherical supramolecular dendrimers are available in Table 3, while additional reconstruction XRD plots are in the Supporting Information. In addition to the values of the lattice dimension a, D_{core}, D_{pore}, and R_{aliph} measured from XRD and fitted, Table 3 also contains the experimental densities (ρ) and number of dendrons, μ, required to self-assemble in the spherical structure.

Chiral and Nonchiral Hollow Spherical Supramolecular Dendrimers. The self-assembly of **1**, **4**, **5**, **9**, and **10** was monitored by a combination of variable-temperature CD and UV−vis spectroscopy similar to the technique used to investigate the self-assembly of the tapered constitutional isomer (4-3,4-3,5)12G2-CH_2-Boc-L-Tyr-L-Ala-OMe.[13] In addition to the experiments carried out in solution (Figure 10), film experiments that support a similar structure in solution and in bulk were also performed (Figure SF13 in Supporting Information). In all cases the UV−vis analysis in solution demonstrates a self-assembly process similar to that observed for the constitutional isomeric dendritic dipeptide into helical pores.[13a] However, only the CD of **1**, at high temperatures (62−90 °C) in molecular solution, shows the Cotton effect of the dipeptide, while at low temperatures (10−60 °C) the transfer of stereochemical information from the stereocenter of the dipeptide to that of a supramolecular chiral object generated from the aromatic part of the dendritic building block (Figure 10a). For this case, CD and UV spectra in solution and in film (Figure SF14 in Supporting Information) are similar to those observed in the case of porous assemblies.[13a] Interestingly, the similarities in

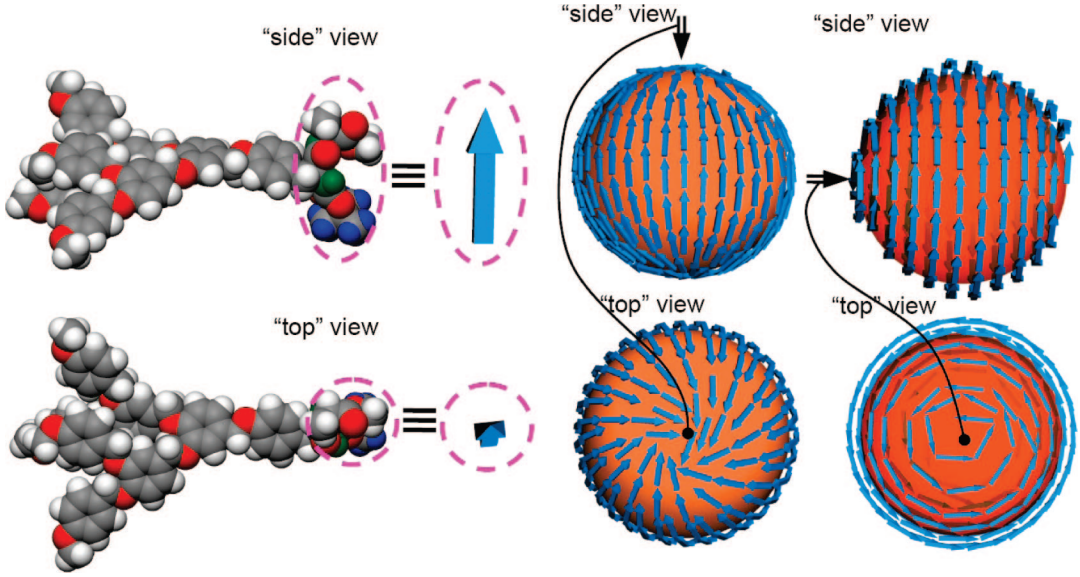

Figure 12. Schematic of the two possible spherical helix or apple peel contours created by the dipeptide on the hollow core of the supramolecular sphere assembled from **1**. The dipeptide is schematically illustrated by an arrow.

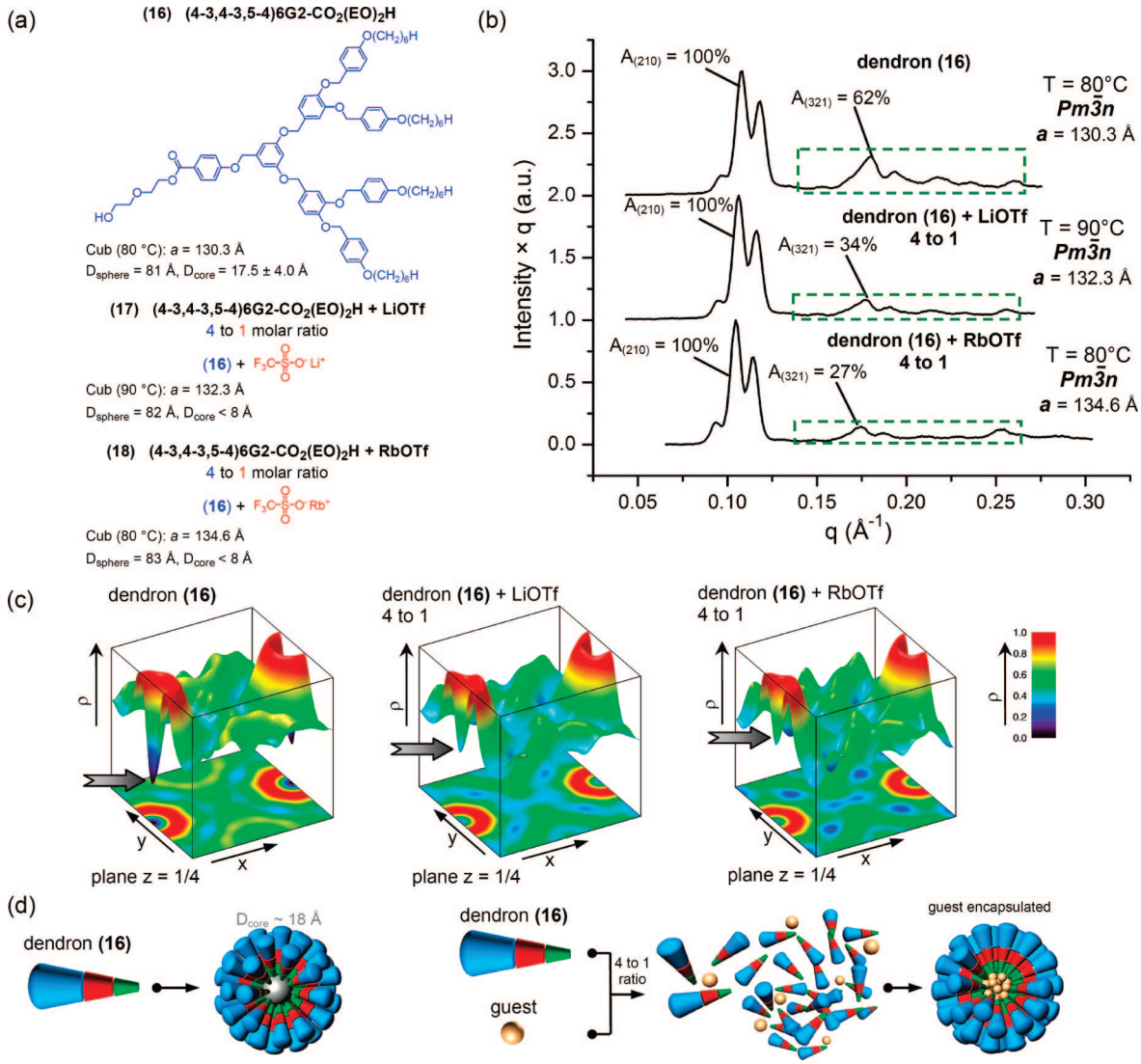

Figure 13. (a) Structure of (4-3,4-3,5-4)6G2-$CO_2(EO)_2H$ (**16**) and structural analysis of its hollow spherical supramolecular dendrimer and its complexes with LiOTf and RbOTf. (b) Small-angle powder XRD and (c) relative electron density maps of the compounds from panel a. (d) Schematic representation of encapsulation of LiOTf and RbOTf guests in the hollow core of the supramolecular sphere assembled from **16**. Representative diffraction peak relative amplitudes are marked in panel b.

the CD spectra of **1** and of its constitutional isomeric (4-3,4-3,5)12G2-CH_2-Boc-L-Tyr-L-Ala-OMe demonstrate a similar handedness of the supramolecular sphere (Figure 10a) and of the porous column (Figure 2 from ref 13a; Figure SF12 in Supporting Information). Therefore, chiral and nonchiral hollow supramolecular spheres self-assemble from chiral dendrons. The chiral dendritic dipeptides self-assemble into chiral hollow spheres, while the chiral dendrons containing stereocenters in the alkyl groups assemble into nonchiral hollow spheres.

Retrostructural Analysis and Models for Chiral and Nonchiral Hollow Spherical Supramolecular Dendrimers. In the case of columnar assemblies, due to their anisotropic structure, powder and fiber XRD experiments performed at both small and wide angles provide information about the lattice dimensions, internal order, and helical structure.[13] The $Pm\bar{3}n$ cubic lattice has three-dimensional periodicity. Therefore, fiber experiments provide access to a large monodomain single-crystal diffractogram[5g] but, due to overlapping, they do not provide information at wide angles related to the helical structure of the chiral or achiral spheres. In cubic phases the most valuable structural and retrostructural information is extracted from small-angle powder XRD experiments (Tables 2 and 3). It is remarkable to observe from the data of Table 3 that the number of dendrons (μ) required to self-assemble into a hollow spherical dendrimer is extremely large, varying between a minimum of 73 (for the $Pm\bar{3}n$ lattice of **4**) and a maximum of 155 dendrons per sphere (for spheres forming the $Pm\bar{3}n$ periodic array of **11**). These large μ values suggest that only conical (Figure 7) dendron conformations are able to assemble into hollow spheres that self-organize in a $Pm\bar{3}n$ cubic lattice.

Figure 11a shows that a fully extended all-trans conical conformation of the dendron **11** placed in a supramolecular spherical dendrimer requires a hollow center with $D_{core} \geq 12.3$ Å to accommodate the experimental $D_{sphere} = 82.2$ Å. This result is very important, since it directly demonstrates the presence of a hollow center. Moreover, it provides a numerical lower bound for the core diameter. Since the alkyl tails of the dendron are not in an all-trans conformation, an experimental value of $D_{sphere} = 82.2$ Å is generated with an experimental $D_{core} = 26.4 \pm 4.0$ Å (Table 3). This model accounts for the assembly of hollow spherical supramolecular dendrimers that self-organize in the cubic lattice (Figure 11b,c). In the nonchiral arrangements

from Figure 11, the conical dendrons do not have any preferential arrangement in the hollow supramolecular sphere. However, when the dendritic dipeptides self-assemble into a hollow sphere, the dipeptide coat of the hollow core is stabilized via intermolecular H-bonding, most probably in a manner similar to that of the helical porous columns.[13a] Figure 12 illustrates a potential mechanism of assembly of a helical dipeptide cavity. An intramolecularly self-folded dendron conformation (Figure 12, left side) is required to mediate the assembly of 155 conical dendrons ($\mu = 155$) into the hollow sphere. The dipeptide adopts a helical arrangement related to that observed in porous columns[13a] except that in the sphere the helical arrangement is more difficult to assemble, and therefore, it requires the introduction of intramolecular disclinations as structural defects (Figure 12, right side). The helical contour shown on the right side of Figure 12 is generated by the dipeptide from the apex of the conical dendritic dipeptide and resembles the path of a spherical helix, also known as loxodrome or rhumb.[19] The spherical helix contour is similar to that of an apple peel. The contour or path of the spherical helix jackets the cage of the hollow spherical supramolecular dendrimer and is responsible for the CD activity shown in Figure 10. This spherical helix cavity resembles recent examples of synthetic molecular apple peels that provide molecular example of chiral capsules.[20] The chiral structure described here represents only one of several models that can be considered. We must remember that the spherical-like structures may be simplified versions of polygonal-like dodecahedral or icosahedral clusters that could explain chirality via alternative mechanisms.

Encapsulation of LiOTf and RbOTf in the Cavity of a Hollow Spherical Supramolecular Dendrimer. Previously it was reported that the attachment of crown ether[21a−c] and oligo(oxyethylene)[21d−g] receptors to the apex of self-assembling dendrons mediates their self-assembly and the encapsulation of LiOTf, NaOTf, and KOTf complexes with oligo(oxyethylene) or polyelectrolytes in the center of supramolecular columns or spheres. Encapsulation of an identical concentration of LiOTf and RbOTf in the center of a supramolecular hollow sphere assembled from dendrons containing oligo(oxyethylene) receptors is expected to increase the electron density at the core region and, therefore, to reduce the amplitude of the higher-order XRD peaks. Figure 13a shows the structure of the dendron (4-3,4-3,5-4)6G2-$CO_2(EO)_2H$ (**16**) that was synthesized in order to perform these experiments. Structural analysis of its hollow spherical supramolecular dendrimer before and after encapsulation of LiOTf and RbOTf are shown in Figure 13a. Synthesis of **16** and its complexation with LiOTf and RbOTf were performed as reported previously[21d−g] and are detailed in the Supporting Information. Figure 13b displays the XRD of **16**, **16**/LiOTf = 4/1, and **16**/RbOTf = 4/1. Incorporation of CF_3SO_3Li salt reduces the amplitude of higher-order diffraction peaks (Figure 13b). Due to its higher number of electrons, the complex of **16** with RbOTf shows an even larger reduction of the amplitude of the XRD peaks. Reconstructed electron density maps of these compounds are shown in Figure 13c. Arrows in Figure 13c indicate significant increases of relative electron density at the center of supramolecular spherical dendrimers. These results confirm the presence of a hollow core and demonstrate the encapsulation. Figure 13d illustrates the encapsulation process. These preliminary encapsulation experiments support the hollow structure of the spherical supramolecular dendrimer and its structural analysis by reconstruction of XRD.

Conclusions

Synthesis and structural and retrostructural analysis of the first library of conical dendrons that self-assemble into hollow supramolecular dendrimers are reported, together with a method to identify and calculate the diameter of the hollow core of supramolecular spheres that self-organize in a $Pm\bar{3}n$ cubic lattice. The simplest strategy to design a self-assembling conical dendron that self-organizes into a hollow sphere is to attach a dipeptide at the apex of a conical dendron. This concept was demonstrated by synthesis of a conical dendritic dipeptide that is a constitutional isomer of the tapered dendritic dipeptide that facilitated the discovery of supramolecular porous columns.[13a] The contour of the shell of the hollow supramolecular sphere self-assembled from the dipeptide moiety resembles the path of a spherical helix or apple peel and is chiral. Alternative methods to design hollow spheres involved the incorporation of one or two additional benzyl ether units at the apex of tapered dendrons to generate conical dendrons that self-assemble into nonhelical spheres. Some of these dendrons self-assemble at lower temperature in porous columns and at higher temperature in hollow spheres. A conical dendron containing a diethylene glycol receptor at the apex was used to encapsulate LiOTf and RbOTf in the hollow core of the supramolecular sphere. These encapsulation experiments were analyzed by XRD, and together with lattice dimensions and structural analysis, they demonstrate the hollow supramolecular structure. The chiral hollow spherical dendrimers reported here resemble biological hollow proteins[17,18] and nonbiological examples of chiral[20,22] and nonchiral[23] supramolecular and molecular[24] capsules. These hollow spheres

(19) (a) Alexander, J. *Math. Mag.* **2004**, *77*, 349–356. (b) Thompson, D. A. W. *On Growth and Form*; Cambridge University Press: Cambridge, U.K., 1961; Vol. 172, p 201.
(20) (a) Garric, J.; Léger, J.-M.; Huc, I. *Angew. Chem., Int. Ed.* **2005**, *44*, 1954–1958. (b) Garric, J.; Léger, J.-M.; Huc, I. *Chem.—Eur. J.* **2007**, *13*, 8454–8462. (c) Bao, C.; Kauffmann, B.; Gan, Q.; Srinivas, K.; Jiang, H.; Huc, I. *Angew. Chem., Int. Ed.* **2008**, *47*, 4153–4156.
(21) (a) Percec, V.; Johansson, G.; Heck, J.; Ungar, G.; Batty, S. V. *J. Chem. Soc., Perkin Trans 1* **1993**, 1411–1420. (b) Johansson, G.; Percec, V.; Ungar, G.; Abramic, D. *J. Chem. Soc., Perkin Trans 1* **1994**, 447–459. (c) Percec, V.; Johansson, G.; Ungar, G.; Zhou, J. *J. Am. Chem. Soc.* **1996**, *118*, 9855–9866. (d) Percec, V.; Cho, W.-D.; Ungar, G.; Yeardley, D. J. P. *Chem.—Eur. J.* **2002**, *8*, 2011–2025. (e) Percec, V.; Heck, J.; Tomazos, D.; Falkenberg, F.; Blackwell, H.; Ungar, G. J. *Chem. Soc., Perkin Trans 1* **1993**, 2799–2811. (f) Percec, V.; Heck, J.; Tomazos, D.; Ungar, G. *J. Chem. Soc., Perkin Trans 2* **1993**, 2381–2388. (g) Percec, V.; Tomazos, D.; Heck, J.; Blackwell, H.; Ungar, G. *J. Chem. Soc., Perkin Trans 2* **1994**, 31–44.
(22) Rivera, J. M.; Martin, T.; Rebek, J., Jr *Science* **1998**, *279*, 1021–1023.
(23) (a) de Mendoza, J. *Chem.—Eur. J.* **1998**, *4*, 1373–1377. (b) Rowan, A. E.; Elemans, J.; Nolte, R. J. M. *Acc. Chem. Res.* **1999**, *32*, 995–1006. (c) Hof, F.; Craig, L.; Nuckolls, C.; Rebek, J., Jr *Angew. Chem., Int. Ed.* **2002**, *41*, 1488–1508. (d) Rudkevich, D. M. *Angew. Chem., Int. Ed.* **2004**, *43*, 558–571. (e) Lutzen, A. *Angew. Chem., Int. Ed.* **2005**, *44*, 1000–1002. (f) Schramm, M. P.; Rebek, J., Jr *Chem.—Eur. J.* **2006**, *12*, 5924–5933. (g) Rebek, J., Jr *Angew. Chem., Int. Ed.* **2005**, *44*, 2068–2078.
(24) (a) Cram, D. J. *Nature* **1992**, *356*, 29–36. (b) Seidel, S. R.; Stang, P. J. *Acc. Chem. Res.* **2002**, *35*, 972–983. (c) Fiendler, D.; Leung, D. H.; Bergman, R. G.; Raymond, K. N. *Acc. Chem. Res.* **2005**, *38*, 351–360. (d) Fujita, M.; Tominaga, M.; Hori, A.; Therrien, B. *Acc. Chem. Res.* **2005**, *38*, 371–380. (e) Cronin, L. *Angew. Chem., Int. Ed.* **2006**, *45*, 3576–3578.
(25) (a) Jansen, J. F. G. A.; De Brabander-van der Berg, E. M. M.; Meijer, E. W. *Science* **1994**, *266*, 1226–1229. (b) Jansen, J.; Meijer, E. W.; De Brabander-van der Berg, E. M. M. *J. Am. Chem. Soc.* **1995**, *117*, 4417–4418. (c) Morgan, M. T.; Carnahan, M. A.; Immoos, C. E.; Ribeiro, A. A.; Finkelstein, S.; Lee, S. J.; Grinstaff, M. W. *J. Am. Chem. Soc.* **2003**, *125*, 15485–15489.

act as dendritic supramolecular capsules that are complementary to the dendritic box.[25] In addition, they represent the first examples of synthetic capsules that undergo reversible shape change from hollow sphere to porous column. Last but not least, these structures have the potential to expand the synthetic and practical opportunities of dendrons, dendrimers, and self-assembling dendrons.[1,4,26]

(26) For selected reviews on supramolecular dendrimers self-organized in lattices, see. (a) Zimmerman, S. C. *Curr. Opin. Colloid Interface Sci.* **1997**, *2*, 89–99. (b) Fischer, M.; Vögtle, F. *Angew. Chem., Int. Ed.* **1999**, *38*, 885–905. (c) Emrick, T.; Fréchet, J. M. J. *Curr. Opin. Colloid Interface Sci.* **1999**, *4*, 15–23. (d) Schlenk, C.; Frey, H. *Monatsh. Chem.* **1999**, *130*, 3–14. (e) Smith, D. K.; Diederich, F. *Top. Curr. Chem.* **2000**, *210*, 183–227. (f) Guillon, D.; Deschenaux, R. *Curr. Opin. Solid State Mater. Sci.* **2002**, *6*, 515–525. (g) Rudick, J. C.; Percec, V *New J. Chem.* **2007**, *31*, 1083–1096. (h) Donnio, B.; Guillon, D. *Adv. Polym. Sci.* **2006**, *201*, 45–155.

Acknowledgment. Financial support by the National Science Foundation (DMR-0548559 and DMR-0520020) and the P. Roy Vagelos Chair at Penn is gratefully acknowledged. We also thank Professor G. Ungar from the University of Sheffield for reading the manuscript and for constructive suggestions.

Supporting Information Available: Experimental synthetic procedures with complete spectral, structural, and retrostructural analysis. This material is available free of charge via the Internet at http://pubs.acs.org.

JA8034703